Rev. Mexicana Astron. Astrof., 13, 41-48 (1986)

OBSERVATIONAL CONSTRAINTS TO THEORETICAL MODELS FOR TYPE I SUPERNOVAE

R. López [1], J. Isern[1,2] and J. Labay[1]
Departamento de Física de la Tierra y del Cosmos
Universidad de Barcelona, España

and

R. Canal[2]
Departamento de Astrofísica
Universidad de Granada, España

Received 1985 December 22

RESUMEN

Generalmente se cree que las supernovas de Tipo I son el resultado de la explosión de una enana blanca masiva, que forma parte de un sistema estelar doble. Las propiedades de las curvas de luz, así como la correlación propuesta por Pskovskii y Branch sugieren que tales explosiones deben dejar un residuo en algunos casos. Esta condición se cumple de forma natural si se toma en consideración que la enana blanca puede tener un núcleo sólido y que la ignición termonuclear comienza en el borde de éste.

En este trabajo se comparan las curvas de luz observadas con las teóricas obtenidas de la explosión de enanas blancas parcialmente sólidas para un amplio rango de los parámetros relevantes. Nuestros resultados muestran que el carácter "lento" y "rápido" de la curva de luz depende básicamente del material expulsado (M_{ej}) y de la fracción de este material que no ha sido procesado hasta el equilibrio estatístico nuclear (M_δ). Las observaciones limitan los valores de estos parámetros al rango $0.8\ M_\odot \leqslant M_{ej} \leqslant 1.4\ M_\odot$ y $0.2\ M_\odot \leqslant M_\delta \leqslant 0.4\ M_\odot$. El valor de la constante de Hubble $H_0 = 100$ km s^{-1} Mpc^{-1} parece estar excluido para cualquiera de los valores razonables de los parámetros de nuestros modelos.

ABSTRACT

It is generally thought that Type I supernovae are the outcome of the explosion of a massive white dwarf in a close binary system. The properties of the light curves as well as the Pskovskii-Branch effect suggest that such explosions should leave a bound remnant in some cases. This condition is naturally fulfilled by taking into account that the white dwarf may have a solid core and that the thermal runaway starts at the edge of this core.

In this paper, observed light curves are compared with the theoretical ones obtained from the explosion of partially solid white dwarfs for a wide range of the relevant parameters. Our results show that the "slow" and "fast" character of the light curve depends basically on the expelled material (M_{ej}) and on the fraction of this material that has not been processed to the nuclear statistical equilibrium (M_δ). The observations constrain these parameters to take values in the range $0.8\ M_\odot \leqslant M_{ej} \leqslant 1.4\ M_\odot$ and $0.2\ M_\odot \leqslant M_\delta \leqslant 0.4\ M_\odot$. A value of the Hubble constant $H_0 = 100$ km s^{-1} Mpc^{-1} seems to be excluded for any reasonable choice of the relevant parameters of our models.

Key words: STARS-WHITE DWARFS – SUPERNOVAE

I. INTRODUCTION

It is usually thought that Type I supernova explosions (SNI) originate from the thermonuclear deflagration of a carbon-oxygen white dwarf, member of a close binary system. Mass accretion on the white dwarf pushes it towards the Chandrasekhar limit and induces explosion. Wide acceptance of this scenario arises from the fact that it qualitatively reproduces the observed characteristics of SNI.

Current models assume the explosion of massive white dwarfs ($M = 1.2$ to $1.4\ M_\odot$). Numerical simulations trying to reproduce SNI explosions predict incineration to ^{56}Ni of about $1\ M_\odot$ of the star. Most of the energy liberated by the explosion comes out as kinetic energy of the expanding material. The velocities calculated for the external layers (Sutherland and Wheeler 1984) are comparable to those actually observed (Kirshner 1982). Decays of ^{56}Ni to ^{56}Co and of ^{56}Co to ^{56}Fe give enough energy to power the light curve. The observed shape of the light curves agrees with the predicted behaviour (Barbon, Ciatti, and Rosino 1973; Barbon, Cappellaro,

1. Grup d'Astrofisica de la Societat Catalana de Fisica (Institut d'Estudis Catalans).
2. Instituto de Astrofisica de Andalucía, C.S.I.C., Spain.

and Turatto 1984). Synthetic spectra calculated by Axelrod (1980) actually confirm those models by reproducing reasonably well the spectroscopic observations of SNI at late times. (See Trimble 1982 for a review).

It must be pointed out that there is a subclass of peculiar SNI (Panagia *et al.* 1985; Wheeler and Levreault 1985; Uomoto and Kirshner 1985). It cannot be ascertained, yet, whether the origin of this subclass of SNI is or not the same as that of "classical" SNI. Wheeler (1986) attributes the outburst to collapse and explosion of an intermediate mass star having lost its envelope either by binary mass transfer or by a strong stellar wind. If we leave this "peculiar" subclass aside, we see that the photometric and spectroscopic homogeneity predicted by the deflagration models of a C – O white dwarfs is confirmed by the observational data.

A more detailed analysis shows, nonetheless, a range of variation from one supernova to the other. Pskoskii (1977) and Branch (1982) have found a correlation between luminosity at maximum, expansion velocity, and the rate of decline of the light curve (previous to the exponential tail). The most luminous supernovae expand faster and their luminosity decay more slowly. In contrast, dimmer supernovae expand slower and their post-maximum decline is steeper. This can be quantitatively expressed as:

$$v_9 = 1.2 + 0.05\,(7 - \beta) \qquad (1)$$

(v_9 is the velocity expressed in units of 10^9 cm s^{-1})

$$M_B = -21.03 + 0.11\,\beta \qquad (2)$$

The dispersions being ±800 km s^{-1} and $\pm 0^m.5$, respectively. The parameter β is defined as the ratio of the magnitude difference between the magnitudes at maximum and at the beginning of the exponential tail to the corresponding time difference. It is expressed as magnitudes per 100 days. The observed values fall into the range $6 \leqslant \beta \leqslant 14$.

Thermonuclear deflagration models of C – O white dwarfs, predicting complete disruption of the star, do account for the general feature of "classical" SNI, but they are unable to reproduce the Pskovskii-Branch effect. López *et al.* (1986) show how this effect could be explained, with the explosion leaving a bound remnant. The possibility of leaving such a bound remnant arises from the fact that C – O white dwarfs in close binary systems are, in general, solid objects. The consequences of solidification have been largely explored by Isern *et al.* (1983) and references therein. Depending on the size of the solid core at the onset of the thermal runaway, these models predict either the total disruption or the formation of a bound remnant (a neutron star or a white dwarf) (Canal *et al.* 1986).

Numerical, self-consistent simulation of a white dwarf explosion is rather a complex, time-consuming calculation. It involves treatment of burning front propagation, the nuclear reaction network, shock wave formation, etc. In the present paper we only intend to explore the minimal requirements to be fulfilled by the theoretical models of SNI explosions in order to be compatible with the observational data.

II. RESULTS AND DISCUSSION

We have constructed models for SNI light curves following the procedure described in López *et al.* (1986). Those models assume thermonuclear explosion of a compact object. Both, the amount of material ejected and the mass of ^{56}Ni synthesized are variable. The explosion energy is spent on gas expansion, while radioactive decay of ^{56}Ni accounts for the light curve. The models only cover the stages previous to the exponential "tail".

a) *Models leaving no Bound Remnant*

The two basic parameters governing the shape of a SNI light curve are the amount of matter ejected and that of ^{56}Ni synthesized. Most models proposed so far give total disruption of the star. The ejected mass is approximately equal to the Chandrasekhar mass.

Those models treat the white dwarf's interior as being fluid. Burning front propagation through fluid layers is still an open problem (Wheeler 1982; Müller and Arnett 1985). This introduces a sizeable uncertainty as to the amount of ^{56}Ni synthesized. In order to analyze the implications of this uncertainty on the light curves, we have calculated a first series of models for different values of the ^{56}Ni mass. Their characteristics are shown in Table 1.

M_{Ni}, R_p, v_p, L_{43} and M_B are, respectively, the mass of ^{56}Ni sinthesized, and radius, expansion velocity of photospheric material, bolometric luminosity, and abso-

TABLE 1

MODELS THAT SUFFER TOTAL DISRUPTION

Model	M_{ej} ($M_\odot$)	M_{Ni} ($M_\odot$)	E_{kin} (10^{51} erg)	R_p (10^{15} cm)	V_p (km s^{-1})	L_{43} (erg s^{-1})	M_B
a	1.435	1.2	1.12	1.60	13118	2.26	−20.01
b′	1.435	0.9	0.70	1.69	10247	1.48	−19.44
c′	1.435	0.65	0.36	1.46	7615	0.91	−18.85

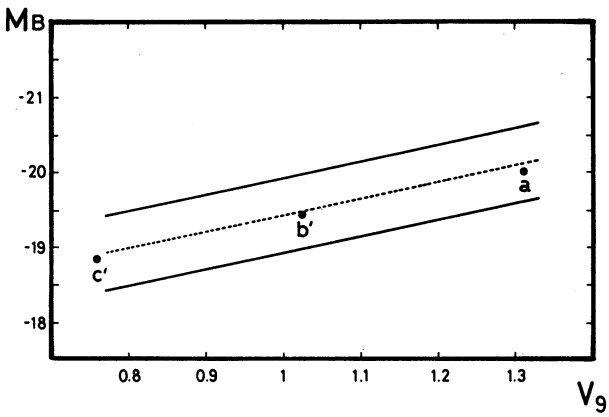

Fig. 1. B-magnitude versus ejection velocity diagram at maximum light for Type I supernovae ("v-M_B diagram" hereafter). The strip is the loci of the observations and the dashed line represents the best fit obtained by Pskovskii assuming $H_0 = 60$ km s^{-1} Mpc^{-1}. Dots correspond to models of Table 1.

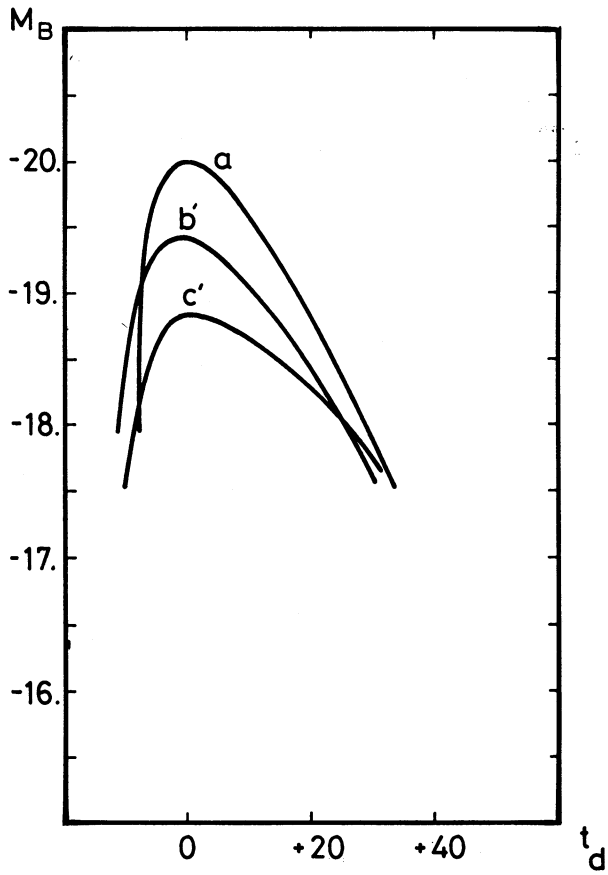

Fig. 2. Light curves for models of Table 1. In these models the white dwarf is completely disrupted.

lute magnitude in the B-band, all at maximum light. E_{kin} is the kinetic energy of the initial models. It is the difference between explosion energy and binding energy. The ejected mass is 1.435 $M_\odot$ in all models. A constant value for the opacity has been adopted $\kappa = 0.2$ cm^2 g^{-1} (Colgate and McKee 1969).

Figure 1 shows the position of the models on an expansion velocity-absolute B-magnitude at maximum diagram. Figure 2 shows the light curves. From both figures we see that the results are compatible with the observed luminosities and expansion velocities and also with the average shape of the light curves. However, changes in the amount of ^{56}Ni alone cannot reproduce the Pskovskii-Branch effect, since the light curves become broader when the maximum luminosity is lowered.

b) *Models with Bound Remnant*

Evolutionary models of mass-accreting white dwarfs have recently been constructed (Labay, Canal, and Isern 1983; Isern *et al.* 1983). Those models include the fact that the white dwarf interior's can be solid and even go through a chemical separation process (Stevenson 1980). In C – O white dwarfs, oxygen settles at the center and carbon is concentrated in the outer layers (Canal, Isern, and Labay 1980; Mochkovich 1983). Calculations show that when the thermonuclear runaway starts there is still a central solid core. Its size depends on the initial mass and the initial temperature of the white dwarf, and on the accretion rate. Outside the core there is a carbon-rich "mantle". The ignition takes place at the base of this mantle (Figure 3). Those models provide a natural way for variation of both the ejected mass and the amount of ^{56}Ni synthesized. The thermonuclear burning front propagates very slowly through the solid layers (Isern, Labay, and Canal 1984). In this case only a fraction of the mantle is burnt into ^{56}Ni and ejected by the explosion. Table 2 shows the characteristics of those models.

A total mass of 1.435 $M_\odot$ has been adopted for the white dwarf, and a value of 0.2 cm^2 g^{-1} for the opacity, the same as for models in Table 1. Figures 4 and 5 show that these models not only agree with the observational data as to expansion velocities, maximum luminosities, and light curve shape, but they also reproduce the Pskovskii-Branch effect. The behaviour of the models in Table 2 can be understood on the basis of the analytical models derived by Arnett (1982). According to them, peak luminosity width scales as $(\kappa\, M_{ej}^3/M_{Ni}^*)^{1/4}$, and the expansion velocity as $(M_{Ni}^*/M_{ej})^{1/2}$, where M_{Ni}^* is the effective amount of ^{56}Ni to be synthesized in order to eject the mantle. Peak luminosity is proportional to ^{56}Ni mass (López *et al.* 1986).

The mass of ^{56}Ni produced not only depends on the size of the oxygen core, but also on the outermost point reached by the burning front. In the fluid phase, the burning front propagates through Rayleigh-Taylor instability and its speed is of the order of the sound speed (Wheeler 1982). Detailed numerical calculations are very complex, given the difficulties arising when mixing NSE material with non-NSE material. For that reason, several authors have either adopted a propagation speed which

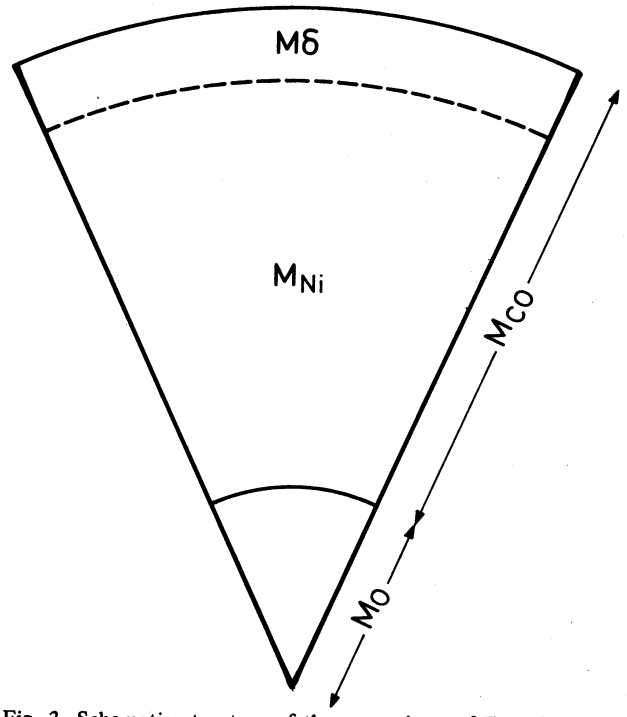

Fig. 3. Schematic structure of the progenitors of Type I supernovae. "M_O" is the solid oxygen core and "$M_{C\text{-}O}$" is the fluid carbon-oxygen mantel. "M_{Ni}" represents the incinerated material and "M_δ" the unburnt part of the star.

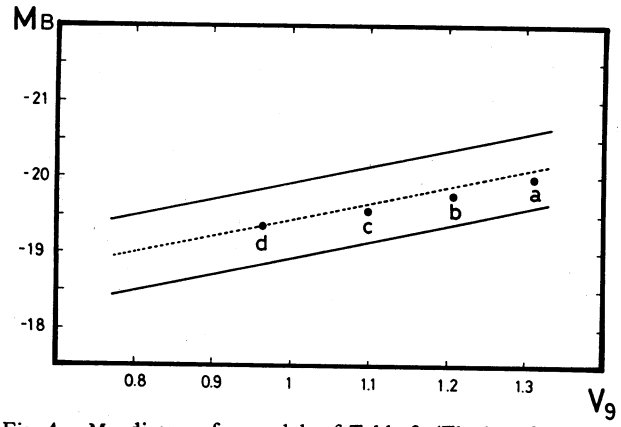

Fig. 4. v-M_B diagram for models of Table 2. (The best fit is also for $H_0 = 60$ km s^{-1} Mpc^{-1}).

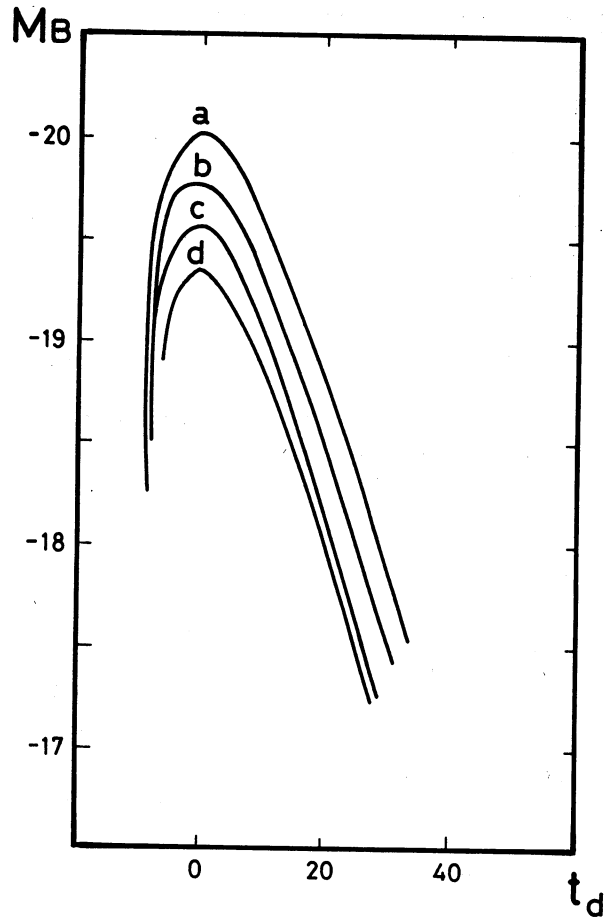

Fig. 5. Light curves for models of Table 2 (models that leave bound remnants).

is a constant fraction of the local sound speed (0.2-0.3), or velocity prescriptions derived from a time-dependent mixing-length theory, where the mixing length is left as a free parameter (Nomoto and Sugimoto 1977). For instance, for $\alpha = 1/H_p$ equal to 0.6, 0.8, 1, and 2, they obtain M_{Ni} equal to 0.49, 0.65, 0.8, and 1.15 $M_\odot$ respectively (Nomoto 1984; Jeffrey and Sutherland 1985). Given those uncertainties, one cannot accurately determine how much of the external mass left unburnt (M_δ). For every value of M_δ, different masses of the central oxygen core have been assumed. We have: $M_{Ni} = M_{tot} -$

TABLE 2

MODELS THAT LEAVE A BOUND REMNANT

Model	M_{ej} ($M_\odot$)	M_{Ni} ($M_\odot$)	E_{kin} (10^{51} erg)	R_p (10^{15} cm)	V_p (km s^{-1})	L_{43} (erg s^{-1})	M_B
a	1.435	1.2	1.12	1.60	13118	2.26	−20.01
b	1.2	1.0	0.81	1.52	12075	1.83	−19.76
c	0.9	0.7	0.50	1.30	10975	1.49	−19.55
d	0.8	0.6	0.34	1.18	9645	1.22	−19.34

TABLE 3

INFLUENCE OF NON-INCINERATED EXTERNAL MASS

Model	M_{ej} ($M_\odot$)	M_{Ni} ($M_\odot$)	E_{kin} (10^{51} erg)	R_p (10^{15} cm)	V_p (km s^{-1})	L_{43} (erg s^{-1})	M_B
			$M_\delta = 0.2$				
a_1	1.435	1.2	1.12	1.60	13118	2.26	−20.01
d_1	0.8	0.6	0.34	1.18	9645	1.22	−19.34
			$M_\delta = 0.3$				
a_2	1.435	1.135	1.05	1.60	12726	2.05	−19.88
d_2	1.0	0.7	0.45	1.35	9958	1.29	−19.36
			$M_\delta = 0.4$				
a_3	1.435	1.0	0.95	1.68	11914	1.87	−19.74
d_3	1.2	0.8	0.63	1.50	10677	1.47	−19.48

$M_\delta - M_{core}$, where $M_{tot} = 1.435\ M_\odot$. Table 3 shows the initial parameters and the characteristics of these models at the peak of the light curve. The quantity of ^{56}Ni in model *d* is the minimun value allowable to reproduce the Pskovskii-Branch effect as to the width of the light curve (López *et al.* 1986). Increasing M_δ reduces the possible combinations of M_{ej} and M_{Ni} which are able to simultaneously produce high luminosities, high velocities, and broad light curves. The corresponding ranges of variation for M_B and v_{ej} finally become narrower than those observed (see Figure 6).

The basic parameters that characterize the light curves are ejected mass and ^{56}Ni mass. There are, however, other physical parameters that can influence the results. Opacity is an important one. Since the gas is far from LTE, its opacity is uncertain. A lower bound to its value comes from the free electrons, whose number depends on the ionization degree of the material. The opacity due to scattering by free electrons in a gas composed by iron-peak elements is $0.007s$, where *s* is the degree of ionization (Chevalier 1981). Since the spectra at times close to maximum light show multiply ionized elements, opacity values above 0.01 cm^2 g^{-1} are generally accepted. As the absorption opacities in those conditions are not reliably known, nor is the importance of the expansion effects on their values (Karp *et al.* 1977), usually adopted values for κ range from 0.08 to 0.2 cm^2 g^{-1} (Colgate and McKee 1969; Arnett 1982; Sutherland and Wheeler 1984). In order to evaluate the influence of the opacity on the light curves, we have recalculated models *a*, *b*, and *c* from Table 2, for $\kappa = 0.1$ cm^2 g^{-1}. The results obtained in this case are displayed in Table 4. Figure 7 shows the positions of the two series of models in the v-M_B diagram. The global effect is an increase by about $0^m.5$ of the maxima and a decrease in the velocities of the layers close to the photosphere by about 700 km s^{-1}. Both changes are of the same order as the observational dispersions of the corresponding values. In the last case ($\kappa = 0.1$ cm^2 g^{-1}), the H_0 value giving the best fit to the models is 50 km s^{-1} Mpc^{-1}. In Figure 8 we show the light curves for models *a* and *a'*. As it should be expected, luminosity decreases with increasing opacity and, as shown by the scaling relationship above, light curves become broader. Also, the rise to maximum is steeper for lower opacities. Besides, since Ni is not observed at maximum light, were the opacity lower than 0.1 cm^2 g^{-1}, one should exclude the models with M_δ, the non-incinerated mass, below $0.2\ M_\odot$.

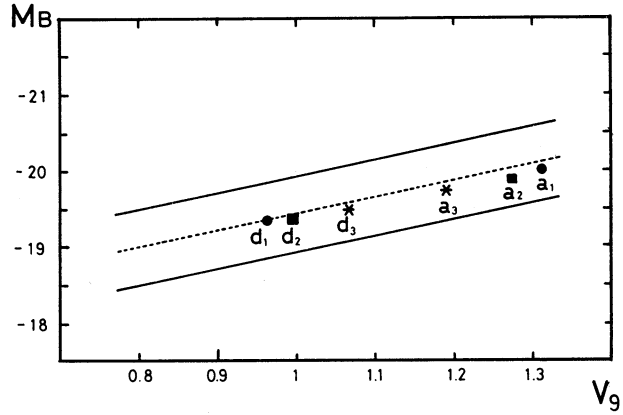

Fig. 6. Influence of the non-incinerated mass of the white dwarf (M_δ) on the position of Type I supernovae in the v-M_B diagram. Dots correspond to models with $M_\delta = 0.2\ M_\odot$, squares to models with $M_\delta = 0.3\ M_\odot$ and asterisks to models with $M_\delta = 0.4\ M_\odot$. In all cases, models labelled with "a" do not leave bound remnants, and the mass of ^{56}Ni synthesized in models "d" is the minimum that is required to reproduce the "Pskovskii-Branch" effect.

In all the models considered so far the total mass of the white dwarf has the same value. But thermonuclear ignition can happen at slightly different central densities ($3 \times 10^9 \leqslant \rho_{ig} \leqslant 10^{10}$ g cm^{-3}), which also means slightly different total masses. That changes the binding energies and thus the amount of nuclear energy available for

TABLE 4

INFLUENCE OF THE VALUE OF THE OPACITY

Model	M_{ej} ($M_\odot$)	M_{Ni} ($M_\odot$)	E_{kin} (10^{51} erg)	R_p (10^{15} cm)	V_p (km s^{-1})	L_{43} (erg s^{-1})	M_B
a	1.435	1.2	1.12	1.60	13118	2.26	−20.01
a′	1.435	1.2	1.12	1.26	12745	2.93	−20.41
b	1.2	1.0	0.81	1.52	12075	1.83	−19.76
b′	1.2	1.0	0.81	1.16	10788	2.37	−20.18
c	0.9	0.7	0.50	1.30	10975	1.49	−19.55
c′	0.9	0.7	0.50	0.99	10095	1.89	−19.94

Models a, b, and c: $\kappa = 0.2$ cm^2 g^{-1}. Models a′, b′, and c′: $\kappa = 0.1$ cm^2 g^{-1}.

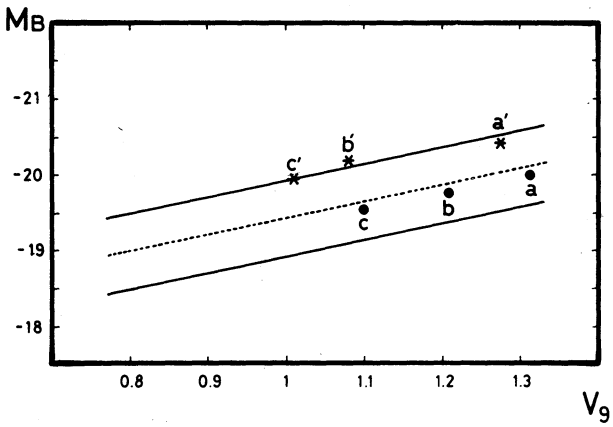

Fig. 7. v-M_B diagram for models of Table 4. Dots correspond to models with an opacity $\kappa = 0.2$ cm^2 g^{-1}. Asterisks to same models with $\kappa = 0.1$ cm^2 g^{-1}. In the last case, the best fit to the Pskovskii-Branch relationship is obtained assuming $H_0 = 50$ km s^{-1} Mpc^{-1}.

expanding the material, the so-called "effective Ni mass" (the total mass of Ni produced minus the equivalent to the binding energy). In order to evaluate the corresponding changes in the light curves, we have calculated three more models, for ignition densities 3×10^9, 7.55×10^9, and 1.05×10^{10} g cm^{-3}, in the case of total disruption of the white dwarf. Results show that luminosity and light curve shape are hardly affected and the expansion velocities alone are slightly modified. Their variations remain below 500 km s^{-1}, and thus are within the observed dispersion. The positions of those models in the v-M_B diagram indicate a better agreement with the Pskovskii-Branch effect for the models where ignition happens at higher densities (model *a*: $\rho_{ig} = 10^{10}$ g cm^{-3}).

We have always assumed that the whole nuclear energy available is converted into kinetic energy of expansion. There are, however, several factors that can modify this hypothesis. Electron captures on the incinerated material generate copious amounts of neutrinos, taking away a fraction of the available energy with them. Also, incineration may be incomplete in the outermost layers and thus the total energy released would be lower. In order to elucidate the importance of those effects, we have calculated another series of models where the energy yield

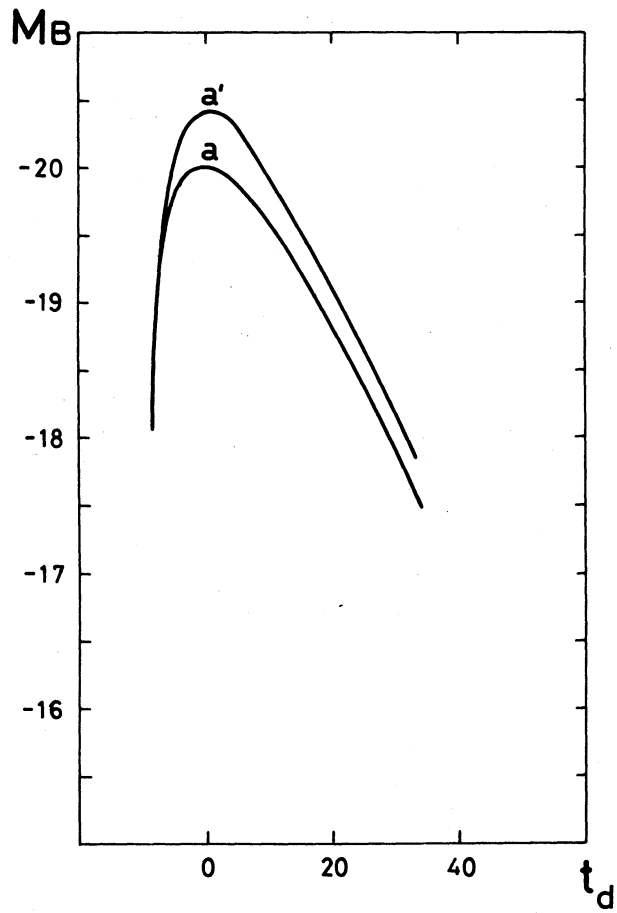

Fig. 8. Light curves for models "a" ($\kappa = 0.2$ cm^2 g^{-1}) and "a′" ($\kappa = 0.1$ cm^2 g^{-1}) of Table 4.

has been parametrized through α, the fraction of the available energy that goes into kinetic energy. In Table 5 we give the characteristics of models calculated for $\alpha = 1$ (models *a*, *c*, and *d*), and for $\alpha = 0.8$ (models *a'*, *c'*, and *d'*). Maximum luminosities are practically unaffected. Expansion velocities are lowered by about 1000 km s^{-1}. Figure 9 shows these effects. Light curves shapes are only slightly broadened. When α lower than 0.8, the models with least ^{56}Ni synthesized would be hardly compatible with the observed velocities.

Calculations by Colgate and McKee (1969) showed that the explosion of a polytropic structure of index n = 3 produces an extended structure composed by an uniform density core which contains about 60% of the initical mass, surrounded by an envelope whose density decreases with the radius as $\sim r^{-p}$, where p takes the value of 6.5 for an initial structure of 1.4 $M_\odot$ and higher values for lower masses. Moreover, numerical models show that the envelopes are quite well fitted by the aforementioned relationship except for the outermost regions which show a steeper dependence (Branch *et al.* 1985). In order to know the influence of the density profile on the light curves, we have computed two models with p = 6.5 and p = 7. In both cases we have assumed that no bound remnant is left. Table 6 shows the characteristics of both models. The main results are the broadening of the light curve, even in the pre-maximum regime, and the reduction of the expansion velocity as p decreases. Steeper profiles than p = 7.5 give expansion velocities that do not agree with the observed ones.

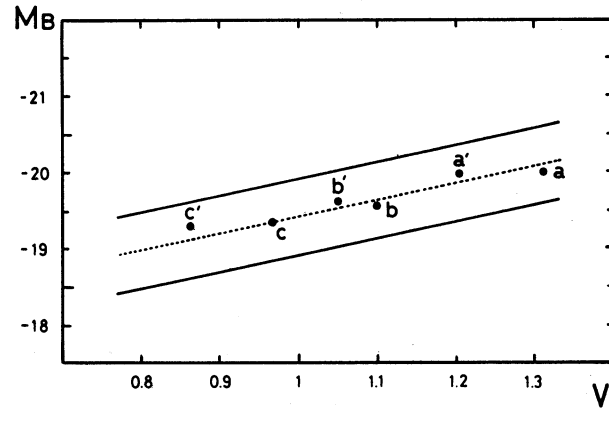

Fig. 9. v-M_B diagram for models of Table 5. Models marked with (') have been calculated assuming $\alpha = 0.8$ (i.e., losses in the thermonuclear energy of about 20%). The ejection velocity is strongly affected by these losses as it can be seen from the figure.

TABLE 5

INFLUENCE OF THE PARAMETER α

Model	M_{ej} ($M_\odot$)	M_{Ni} ($M_\odot$)	E_{kin} (10^{51} erg)	R_p (10^{15} cm)	V_p (km s^{-1})	L_{43} (erg s^{-1})	M_B
a	1.435	1.2	1.12	1.60	13118	2.26	-20.01
a'	1.435	1.2	0.92	1.52	12017	2.20	-20.00
b	1.0	0.8	0.60	1.38	11408	1.61	-19.64
b'	1.0	0.8	0.49	1.29	10508	1.56	-19.62
c	0.8	0.6	0.34	1.18	9645	1.22	-19.34
c'	0.8	0.6	0.27	1.14	8655	1.18	-19.31

Models a, b, and c: $\alpha = 1$. Models a', b', and c': $\alpha = 0.8$.

TABLE 6

INFLUENCE OF THE DENSITY PROFILE

Model	M_{ej} ($M_\odot$)	M_{Ni} ($M_\odot$)	E_{kin} (10^{51} erg)	R_p (10^{15} cm)	V_p (km s^{-1})	L_{43} (erg s^{-1})	M_B
a	1.435	1.2	1.12	1.60	13118	2.26	-20.01
a'	1.435	1.2	0.80	1.50	11789	2.30	-20.05

Model a: p = 7. Model a': p = 6.5.

III. CONCLUSIONS

Generally speaking, thermonuclear deflagration of a white dwarf in a close binary system can reproduce the average characteristics of Type I supernovae. Ordinary models cannot, however, account for the Pskovskii-Branch effect. Attempts have been made to reproduce this effect by only varying the amount of ^{56}Ni generated. Besides being *ad hoc*, this produced an effect that is the opposite to the observed one.

If we take into account that a white dwarf can easily become solid and that in many cases it is still partially solid when thermonuclear ignition happens, the Pskovskii-Branch effect naturally results from this property, since both ejected mass and ^{56}Ni change from an explosion to another. It must be stressed that, in the framework of this last type of models it is not necessary to assume the star to be solid in every case. Only a fraction of the explosions leave bound remnants (when there is still a solid core at ignition). The expected frequency of the outburst is not changed by that (they do not generally have to be delayed until the star has become solid). The recent discovery of a subclass of "peculiar" SNI, whose progenitors might be intermediate-mass star, contributes to the agreement between observed frequencies and theoretical ones (those deduced from the proposed scenarios).

Observational data concerning SNI are still scarce and incomplete. There is still a sizeable dispersion in the values of the maximum luminosities and, specially, in the expansion velocities. In the same way, the criteria foı classifying SNI as either "slow" or "fast" still lack reliability and precision. All the uncertainties put together, we cannot determine the range of the basic parameters of our models in a clear-cut way. The most important one appears to be M_δ, the non-incinerated mass. Its value critically depends on the mode of propagation of the burning front through fluid layers, and this last problem is far from solved. Were M_δ larger than 0.4 $M_\odot$, models assuming off-center ignitions might hardly reproduce the Pskovskii-Branch effect. On the other hand, the presence of intermediate-mass elements moving at high speeds, together with the absence of Ni in the spectra at maximum luminosity, do suggest that the non-incinerated mass, for reasonable values of the opacity ($\kappa = 0.1 - 0.2$ cm^2 g^{-1}), cannot be much lower than 0.2 $M_\odot$. Also, the mass of the thermonuclearly inert core being between 0 and 0.6 $M_\odot$, the losses in the process of conversion of nuclear and internal energies into kinetic energy cannot be larger than about 20%, unless we assume a contribution from gravitational energy (bounce of the compact remnant).

This work has been partially financed by the *CAICYT*, grant 400/84.

REFERENCES

Arnett, W.D. 1982, in *Supernovae: A Survey of Current Research*, ed. M.J. Rees and R.J. Stoneham (Dordrecht: D. Reidel), p. 221.

Axelrod, T.S. 1980, in *Proceedings of the Texas Workshop on Type I Supernovae*, ed. J.C. Wheeler (Austin: University of Texas), p. 80.

Barbon, R., Ciatti, F., and Rosino, L. 1973, *Astr. and Ap.*, **25**, 241.

Barbon, R., Cappelaro, E., and Turatto, M. 1984, *Astr. and Ap.*, **135**, 27.

Branch, D. 1982, in *Supernovae: A Survey of Current Research*, ed. M.J. Rees and R.J. Stoneham (Dordrecht: D. Reidel), p. 267.

Branch, D., Doggett, J.B., Nomoto, K., and Thielemann, F.K. 1985, *Ap. J.*, **294**, 619.

Canal, R., Isern, J., and Labay, J. 1980, *Ap. J. (Letters)*, **241**, L 33.

Canal, R., Isern, J., Labay, J., and López, R. 1986, in 5th Moriond Astrophysics Meeting *Nucleosinthesis and its Implications on Nuclear and Particle Physics*, in press.

Chevalier, R.A. 1981, *Ap. J.*, **246**, 267.

Colgate, S.A. and McKee, C. 1969, *Ap. J.*, **157**, 623.

Isern, J., Labay, J., Canal, R., and Hernanz, M. 1983, *Ap. J.*, **273**, 320.

Isern, J., Labay, J., and Canal, R. 1984, *Nature*, **309**, 431.

Jeffery, D. and Sutherland, P. 1985, *Astr. and Space Sci.*, 109, 277.

Karp, A.H., Lasher, G., Chan, K.L., and Salpeter, E.E. 1977, *Ap. J.*, **214**, 161.

Kirshner, R.P. 1982, in *Supernovae: A Survey of Current Research*, eds. M.J. Rees and R.J. Stoneham (Dordrecht: D. Reidel), p. 1.

Labay, J., Canal, R., and Isern, J. 1983, *Astr. and Ap.*, **117**, L1.

López, R., Isern, J., Canal, R., and Labay, J. 1986, *Astr. and Ap.*, **155**, 1.

Müller, E. and Arnett, W.D. 1985, in *Nucleosynthesis Challenges and New Developments*, eds. W.D. Arnett and J.W. Truran (Chicago: University of Chicago Press), p. 235.

Mochkovich, R. 1983, *Astr. and Ap.*, **122**, 212.

Nomoto, K. 1984, in *Stellar Nucleosynthesis*, eds. E. Chiosi and A. Renzini (Dordrecht: D. Reidel), Vol. **109**, p. 239.

Nomoto, K. and Sugimoto, D. 1977, *Pub. Astr. Soc. Japan*, **29**, 765.

Nomoto, K., Thielemann, F.K., and Wheeler, J.C. 1984, *Ap. J. (Letters)*, **279**, L 23.

Panagia, N. *et al.* 1985, preprint.

Pskovskii, Y.P. 1977, *Soviet Astr.-AJ*, **21**, 675.

Stevenson, D.J. 1980, *J. de Phys. Suppl.*, No. 3, Vol. **41**, p. C2-53.

Sutherland, P.G. and Wheeler, J.C. 1984, *Ap. J.*, **280**, 282.

Trimble, V.L. 1982, in *Supernovae: A Survey of Current Research*, eds. M.J. Rees and R.J. Stoneham (Dordrecht: D. Reidel), p. XV.

Uomoto, A. and Kirshner, R.P. 1985, *Astr. and Ap.*, **149**, L 7.

Wheeler, J.C. 1982, in *Supernovae: A Survey of Current Research*, eds. M.J. Rees and R.J. Stoneham (Dordrecht: D. Reidel), p. 167.

Wheeler, J.C. and Levreault, R. 1985, *Ap. J. (Letters)*, **294**, L 17.

Wheeler, J.C. 1986 in 5*th* Moriond Astrophysics Meeting *Nucleosynthesis and its Implications on Nuclear and Particle Physics*, in press.

R. Canal: Departamento de Astrofísica, Universidad de Granada, Campus de Fuentenueva, 18000 Granada, Spain.
J. Isern, J. Labay, and R. López: Departamento de Física de la Tierra y del Cosmos, Universidad de Barcelona, Avda. Diagonal 645, 08028 Barcelona, Spain.

Rev. Mexicana Astron. Astrof., 13, 49-55 (1986)

KINEMATICAL STUDY OF G 339.2−0.4, S 216, AND THE ARC OF THE PLANETARY NEBULA NGC 3242

M. Rosado

Instituto de Astronomía
Universidad Nacional Autónoma de México

Received 1986 February 3

RESUMEN

Este trabajo tiene como objetivo reportar los datos obtenidos mediante fotografías de banda angosta e interferometría de FP de las nebulosas G 339.2−0.4 y S 216 así como del arco nebular que probablemente esté asociado a la nebulosa planetaria NGC 3242. Los datos así obtenidos refuerzan las sugerencias hechas previamente de que G 339.2−0.4 y S 216 sean consideradas como nebulosas planetarias de gran diámetro aún cuando no se hayan identificado sus estrellas excitadoras. En cuanto al arco centrado en NGC 3242, éste parece estar físicamente asociado a la nebulosa planetaria puesto que ambos objetos tienen velocidades de conjunto similares. Más aún, aunque sea un resultado muy incierto, la velocidad de expansión de este filamento resulta ser inferior a la de la propia nebulosa planetaria.

ABSTRACT

The purpose of this work is to show narrow band filter photographs and FP velocity data on the nebulae G 339.2−0.4 and S 216 and on the nebulous arc presumably associated with the planetary nebula NGC 3242. These data give support to previous suggestions that G 339.2−0.4 and S 216 are two large diameter PN although no obvious exciting stars were found. On the basis of their similar systematic velocities the arc centered in NGC 3242 seems to be physically connected with that PN. Our results, although highly uncertain, show the expansion velocity of the filament to be lower than that of the PN.

Key words: NEBULA-PLANETARY — INTERFEROMETRY — INTERSTELLAR-MATTER

I. INTRODUCTION

Large diameter planetary nebulae (PN) appear to be uncommon among the known planetaries. Indeed, Weinberger *et al.* (1983) estimate that there are only 1% of PN with angular dimensions larger than 10 arcmin; however, more recent studies show that this number can be increased considerably by observations at higher sensitivities (Jewitt, Danielson, and Kupferman 1986). In fact, these objects are difficult to detect or to study because of their low surface brightness, which in addition, introduces the selection effect of observing large objects only when the reddening is low.

These objects have been poorly studied because most of the observers have concentrated their attention on smaller objects of high surface brightness and consequently existing studies on these are scanty (Abell 1966). This situation begins to change and there are now more studies of these objects (Kaler 1981; Schönberner 1981; Weinberger *et al.* 1983; Jewitt *et al.* 1986).

Two types of large diameter PN can be distinguished: single shell PN of large diameter and of low surface brightness and "common" PN surrounded by a faint halo of larger dimensions. The single shell large diameter PN often show high [N II] (λλ 6548, 6584 A)/Hα ratios (Aller 1976), and they have, in general, very faint exciting stars ($\bar{M}$ ranges from 1.2 to 10.9 magnitudes, with a mean M = 8.7 mag; Weinberger *et al.* 1983). This may be the reason why some of them were classified as common H II regions, supernova remnants (SNRs), etc. (see for example Rosado and Kwitter 1982). It is thought that these nebulae are quite old and consequently, they represent the latest observable stages in the evolution of PN, a circumstance which makes them very interesting objects for study. On the other hand, the PN with halos have, in general, an exciting star which is much brighter than the large diameter single shell PN ($\bar{M}$ = 5.2 mag). The proper PN are brighter while the halos are much fainter. Very often, the inner PN shell of these PN with halos, have several components (mostly double shell, etc.). It is believed that these nebulae are younger than the larger diameter single shell PN. Recently, Jewitt *et al.* (1986) have detected halos in 2/3 of a sample of 44 PN studied. This would imply that halos are more common that it was thought. The presence of halos around PN is important because their study should provide insight into the mechanism of formation of a PN.

In this work three such objects are studied: namely the "halo" of the PN NGC 3242 and two other nebulae which are presumed to be large diameter single shell PN, S 216 and G 339.1 −0.4.

II. THE OBSERVATIONS

The material obtained is as follows: monochromatic filter photographs in the Hα, [S II] (λλ6717, 6731 A) and [O III] (λλ5007 A) lines and two Fabry-Pérot (FP) interferograms in the light of Hα of the nebula G 339.2 −0.4; one Hα photograph and one Hα interferogram of regions (of 30 and 11 arcmin of diameter respectively) of the nebula S 216 and monochromatic filter photographs in the light of Hα and [N II] (λ6584 A) and three Hα and [N II] interferograms of the arc which seems to be a part of a large halo around the PN NGC 3242. Tables 1 and 2 give information about the plate characteristics of direct photographs and interferograms respectively.

All our data were obtained using the 2.1-m and 84-cm Cassegrain focus telescopes of the Observatorio Astronómico Nacional at San Pedro Mártir, Baja California Norte, in the same way as described in Rosado (1983). The direct photographs have been obtained by means of a focal reducer (Snyder F/2 objective) coupled with a single stage image tube. Four interference filters have been employed: Hα (λ_0 = 6563 A, $\Delta\lambda$ = 10 A), [S II] (λ_0 = 6719 A $\Delta\lambda$ = 16 A), [O III] (λ_0 = 5018 A, $\Delta\lambda$ = 9.7 A) and [N II] (λ_0 = 6584 A, $\Delta\lambda$ = 10 A). The fiber optics output of the image tube was recorded on 103 a-G films. The scale and angular field of these photographs were about 49 arcsec mm^{-1} and 11 arcmin respectively for observations performed with the 2.1-m telescope and 2 arcmin mm^{-1} and 30 arcmin for observations performed with the 84-cm telescope.

The FP interferometry was carried out with the same equipment used for the photographs but with the addition of a FP étalon. The optical mounting of the étalon corresponds to the "focal reducer" type described in Monnet (1970). The FP étalon used in these observations –different to that used in Rosado (1983)– has a resolving power of 10600 and a linear dispersion of about 20 A mm^{-1}. The measurements and data reductions were performed in the standard way (Courtés 1960). Further description of the measurements and reductions can be found in Rosado *et al.* (1982).

Unfortunately, some of the rings are contaminated by the geocoronal Hα line and the atmospheric OH lines at λ6568.7, 6553.7 and 6577.0 A. Since these lines appear clearly separated from the nebular rings, they could be identified and eliminated.

TABLE 1

CHARACTERISTICS OF THE NARROW BAND INTERFERENCE FILTER PHOTOGRAPHS

Plate number	Region	Filter	Exposure Time (min)	Telescope (mts)
SN 181	G 339.2 – 0.4	Hα	40	2.1
SN 189	G 339.2 – 0.4	[S II]	40	2.1
SN 191	G 339.2 – 0.4	[O III]	40	2.1
SN 143	S 216	Hα	60	.84
SN 300	Halo of NGC 3242	Hα	45	2.1
SN 301	Halo of NGC 3242	[N II]	45	2.1

III. THE INDIVIDUAL NEBULAE

a) *G 339.2 – 0.4*

The nebulosity discovered on the "Mathews Extension" to the Palomar Observatory Sky Survey (*POSS*) plates is described as an arc 6 minutes in diameter (Clark, Caswell, and Green 1975) and it is associated with the radio source G 339.2 – 0.4 of flat spectrum (α = −0.2. The deep red photographs of Zealey, Elliot, and Malin (1979) revealed a complete shell of emission of 6 arcmin in diameter which was thought to be the optical counterpart of a SNR of plerionic type, although van

TABLE 2

CHARACTERISTICS OF THE FP INTERFEROGRAMS[a]

Plate number	Region	Approximate 1950 Coordinates of the Centers		Filter	Exposure Time (min)
SN 310	G 339.2 – 0.4	$16^h41^m50^s$	− 46°04′	Hα	75
SN 318	G 339.2 – 0.4	$16^h41^m50^s$	− 46°04′	Hα	60
SN 250	S 216	$4^h40^m50^s$	+ 46°50′	Hα	60
SN 312	Halo of NGC 3242	$10^h21^m50^s$	− 18°28′	Hα	75
SN 313	Halo of NGC 3242	$10^h21^m50^s$	− 18°28′	[N II]	60
SN 316	Halo of NGC 3242	$10^h21^m50^s$	− 18°28′	[N II]	75

a. Interference Order at Hα = 1060. Telescope: 2.1-m.

den Bergh (1978), on the basis of its diffuse morphology, has discarded the SNR hypothesis and has suggested that this nebula could be a PN.

Murdin, Clark, and Haynes (1979) have investigated the radio and optical properties of this source; they confirm the spectral index $\alpha \cong -0.2$ and they obtain also red and blue spectra of the brightest portion of the nebula. These latter data suggest that the nebula could be a low excitation PN. However, Murdin *et al.* (1979) could not rule out the plerionic-SNR hypothesis due to the lack of kinematical observations. Unfortunately as they did not calibrate the red and blue spectra they could not obtain the reddening from the Balmer decrement.

Our monochromatic photographs in Hα, [S II] and [O III] (Figure 4, Plate) confirm the low values of the [S II]/Hα and [O III]/Hβ line-ratios obtained by Murdin *et al.* (1979) on the brightest portion and extend these conclusions to the whole nebula.

Two FP interferograms in Hα were also obtained. The heliocentric radial velocities are displayed in Figure 1. From these data it can be seen that the nebula does not show any violent motion (such as splittings of the FP profiles) which could support the plerionic-SNR hypothesis. Consequently, the kinematical data seem to confirm the suggestion that G 339.1 −0.4 is a low excitation PN and, in agreement with Bohuski and Smith (1974), that some large diameter PN have unusually low intrinsic velocities of expansion (from 40 to < 10 km s^{-1}). In addition, with the present data, the systemic velocity of the nebula is V_c (LSR) $\cong -28 \pm 6$ km s^{-1}.

In the radial velocity field shown in Figure 1 one can appreciate a tendency of the points of the SW zone to have higher velocities than those of the rest of the nebula. However, the zone of low velocities is not so well defined in order to establish a reliable pattern. It should be interesting to have more data points in order to confirm or reject this suggestion.

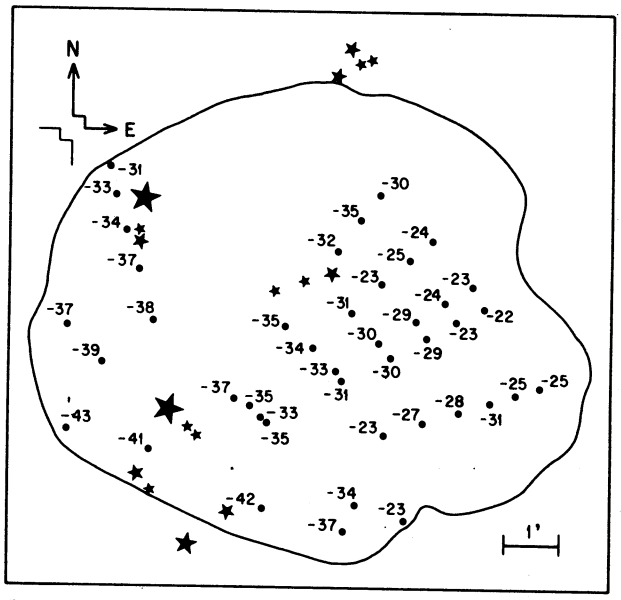

Fig. 1. The heliocentric radial velocity field of G 339.2 − 0.4.

The [S II] λλ6717/6731 line-ratio deduced from the optical spectra (Murdin *et al.* 1979) implies an electron density, n_e, varying from 400 to 2100 cm^{-3} with a mean value of about 1000 cm^{-3}, if an electron temperature of 10^4 °K is assumed and Pradhan (1978) cross sections are used. Furthermore, by using the derived value of n_e and the value of the radio flux at 5 GHz quoted by Murdin *et al.* (1979), $S_{5\ GHz} = 4.5$ Jy, one can obtain the product of the distance (in pc),d, and the fraction of the volume which radiates, ϵ, as follows (Milne and Aller 1975):

$$d\epsilon = 1.7 \times 10^{13} \frac{S}{\theta^3\ n_e^{\ 2}} \qquad (1)$$

where S is the 5 GHz flux in Jy, θ, the angular radius in arcsec and n_e the electron density in cm^{-3}. In obtaining the relation (1) it was assumed that the fraction of He to H, $y = 0.11$, that all the He is singly ionized and that $T_e = 10^4$ °K. By substituting the values corresponding to this nebula: $S = 4.5$, $\theta = 180$ and $n_e = 1000$, one obtains $d\epsilon \cong 13$ pc.

For values of ϵ typical of PN (~ 0.6) one obtains a short distance to this nebula. If this were the case, the exciting star should be easily identifiable which is not the case (see below). On the other hand, another estimate of the distance –or of ϵ– can be inferred if one assumes that the mass of the nebula (supposed to be a PN) is about 0.2 $M_\odot$ (Shklovski method). Thus, under the assumptions of abundances made above:

$$M = (1.3)\ 4/3\ \pi\ R^3\ n_e\ \bar{m}_H\ \epsilon \text{ cgs units} \qquad (2a)$$

$$= (1.3)\ 4/3\ \pi\ \theta_r^3\ d_{cm}^3\ n_e\ \bar{m}_H\ \epsilon \text{ cgs units} \qquad (2b)$$

where $R = \theta_r\ d_{cm}$ is the linear radius of the nebula (in cm), θ_r the radius in radians and d_{cm} in cm, $\bar{m}_H$ the mass of a proton in grams. Since $d\epsilon \cong 13$ pc, in order to have a mass of about 0.2 $M_\odot$ ϵ must be of about 1/30 thus implying a distance of about 400 pc and a linear diameter of about 0.7 pc. At this distance, the nebula deviates from circular motion in an amount V_c (LSR) − V_{ISM} (400 pc) $\cong -22 \pm 6$ km s^{-1} and/or has a mass smaller than the assumed 0.2 $M_\odot$

While the appearance, spectrum and kinematics of this nebula seem to favor the PN interpretation, there remains the problem of identifying the exciting star. Murdin *et al.* (1979) argue that only two stars at the periphery of the nebula have brightness corresponding to the 10th magnitude (among these, a B8 star). The stars found in a circle of about 30 arcsec in radius, centered on the nebula, are considerably fainter (the bright-

est have $m_V > 15$ mag). A search for blue stars was carried out at the center of this nebula by comparing the Hα and [S II] photographs with one in [O III] shown in Figure 4, Plate, a star has been seen in the [O III] photograph that appears extremely faint in the red photographs (unless the faintness could be due to the nearness of the cross-wire in the red photographs). This star is quite faint ($m_V \gtrsim 16$ mag), however, the amount of reddening is not known; placed at a distance of 400 pc, its absolute magnitude would be $M_V \gtrsim 8$ mag. This M_V is in agreement with those of the exciting stars of large diameter PN which have absolute magnitudes varying by about 10 mag (and perhaps more) from the average absolute magnitude of about +8.7 mag (Weinberger *et al.* 1983). Thus, the faintness of the proposed candidate does not seem to be a reason for rejecting it; and it should be interesting to persue its study.

b) *S216*

This nebula, considered to be an H II region by Marsalkova (1974) appeared to have strong [S II] emission relative to the Hα + [N II] emission as the survey of Parker, Gull and Kirshner (1979) has revealed. The [O III] photograph of that survey and an additional [O I] (λ 6300 A) photograph obtained with the same equipment revealed that these emissions are strong, the one in [O III] being concentrated near the center. The object appears as a diffuse circular nebula of 100 arcmin of diameter. Despite its relatively strong [S II] emission, its diffuse appearance and the lack of non-thermal radio emission argue against the assumption of a SNR, although no exciting star had been identified so far as being responsible for the nebular emission.

Fesen, Blair, and Gull (1981) obtained spectra of the brighter eastern portion of the nebula. They were able to obtain the reddening from their observed Hα/Hβ ratios and thus placed an upper limit on the color excess of about 0.5 mag. The observed [S II] (λλ6717/6731) line-ratios suggest $n_e \lesssim 100$ cm^{-3}. From their spectra, it can be ruled out that this nebula is an H II region. In fact, strong lines of [O II] (λ 3727 A), [O III], (λλ4959, 5007 A), [O I] (λ6300 A), [N II] (λλ6548, 6584 A) and [S II] (λλ6717, 6731 A) are present, reminiscent of radiative shock emission or of low ionization PN spectra.

Reynolds (1985) has observed this nebula using a FP interferometer with a field of 49 arcmin and a spectral resolution of 12 km s^{-1}, in the lines of Hα, [N II] and [S II]. He finds an Hα flux of about 8.4×10^{-10} erg cm^{-2} s^{-1}, and confirms that the visual extinction, A_V, cannot be larger than about 1 mag; he obtains LSR systemic velocities in Hα and [S II] of +7.5±1.0 and +9.5±1.8 km s^{-1} respectively and finds no appreciable expansional motion ($V_{exp} \lesssim 4$ km s^{-1}). From several considerations he estimates the distance to the nebula as $d \lesssim 80$ pc. Weinberger *et al.* (1983), estimate also a small distance to this nebula ($d \cong 30$ pc) on the basis of the emission measure estimated from *POSS* plates.

Another estimate of the distance can be obtained by means of the distance scale of Cudworth (1974):

$$d = 108\,\theta^{-3/5}\,F(H\beta)^{-1/5}\ \text{pc}\ , \qquad (3)$$

where θ is the radius in arcsec and F(Hβ) the unreddened Hβ flux in erg cm^{-2} s^{-1}. If S 216 is a PN and that if it is optically thin (as seems to be the case, see Reynold's discussion) putting $\theta = 3000$ and $F(H\beta) = 6.4 \times 10^{-10}$ ($A_V \cong 1$ mag), one obtains $d \cong 60$ pc, which confirms the nearness of this nebula.

In the present work an Hα photograph and an Hα FP interferogram of regions of this nebula have been obtained; Figure 5, Plate shows the Hα photograph and Figure 2 the radial velocity field. No appreciable internal motions are detected from these data. The LSR systemic velocity obtained is V_c (LSR) = 13± 4 km s^{-1}. Both results are in agreement with those of Reynolds (1985). At a distance of about 80 pc, the nebula has a peculiar velocity relative to the surrounding interstellar matter (ISM) –the deviation of the nebular velocity from galactic circular motion– of about 10 km s^{-1} and its linear diameter is supposed to be about 2.4 pc, somewhat typical of large PN (Weinberger *et al.* 1983).

c) *The "Halo" of NGC 3242*

The PN NGC 3242, classified by Kaler (1974) as a double ring PN, shows in addition, a faint nebulous arc located about 10 arcmin southwest of the PN that was first noted by Minkowski (1965, private communication to T.K. Menon). This arc seems to be associated with the PN itself as its center coincides with the PN and

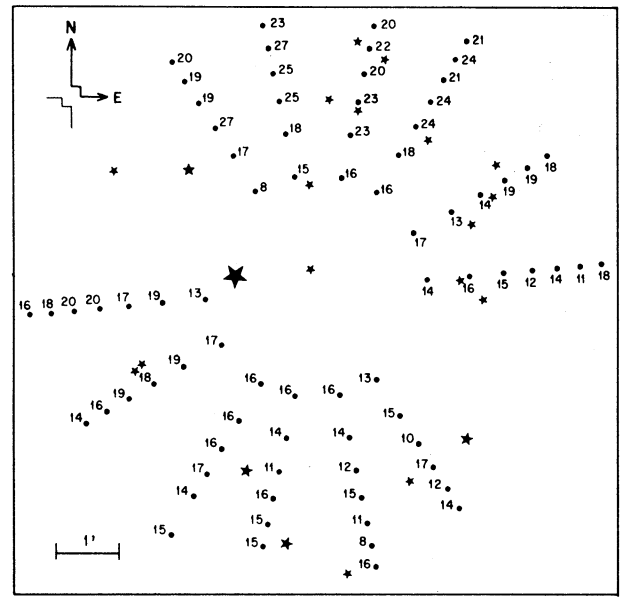

Fig. 2. The heliocentric radial velocity field of a region of S 216.

also because the radio maps at 1400 MHz reveal a clear connection between the optical nebulous arc and the radio contours (Kaftan-Kassim 1966). Later on, Bond (1981) by inspection of the *POSS* prints, had found that a faint nebulosity (of which the brightest portion is the arc) entirely surrounds the PN. Bond has suggested that this nebulosity could be an elliptical halo of the PN with dimensions of about 18 X 24 sq. arcmin and, consequently, NGC 3242 could be classified as a giant PN with halo (following Kaler's (1974) designation). Weinberger *et al.* (1983) were not able to identify the reported halo around the PN; however, the presence of the filament points towards this idea while, on the other hand, the dimensions quoted by Bond (1981) must be taken as highly uncertain. With respect to the PN, it shows a double ring morphology, being the dimensions of the inner and outer rings of about 15.2 and 38 arcsec respectively. The PNN shows a continuum spectrum; however, in the *UV* one might identify some P Cygni profiles, an evidence that the PNN has stellar winds (Cerruti-Sola and Perinotto 1985). These authors assign $T_{eff} \cong 89125$ °K and $L_* = 10^3\ L_\odot$ as the effective temperature and the luminosity of the PNN, respectively.

Values of the distance to NGC 3242 range from 0.787 kpc (Maciel and Pottasch 1980) to 1.697 kpc (Cudworth 1974). Spectroscopic work on this nebula has been performed by Barker (1978) who finds that the [O III] emission is quite large relative to Hβ while the [N II] and [S II] emissions are much fainter than Hα. The tables of Sabbadin and Minello (1978) show similar line-ratios. The electron density obtained from these spectroscopic studies are of about 2×10^3 cm^{-3}. The estimated mass of this PN is about 0.18 $M_\odot$ if a distance of 1.697 kpc is assumed (Sabbadin and Minello 1978). On the other hand, the Hβ flux reported by Milne and Aller (1975) of 1.7×10^{-10} erg cm^{-2} s^{-1} permits to determine the rms electron density. By taking an $E(B-V) = 0.15$ mag (Milne and Aller (1975), an angular diameter of 38 arcsec and by assuming a case B photoionized nebula with $T_e = 10^4$ °K (Osterbrock 1974) one obtains that $\epsilon\ n_e$ ranges from 1.7×10^3 to 2.5×10^3 cm^{-3} according with the difference in the assumed distance (from 1.697 to 0.787 kpc respectively). Thus, ϵ, the fraction of the volume which radiates is $\lesssim 1$.

Kinematical studies of the central PN have been performed by Wilson (1950), Weedman (1968) and Welty (1983). These authors report different values of the heliocentric systemic velocity of this PN, $V_\odot$(PN). The mean of these values is adopted and consequently, $V_\odot$ (PN) = 6.3±2 km s^{-1}. On the other hand, the value of the expansional velocity of the PN, V_{PN}, reported by Wilson (1950) and Welty (1983) is of about 22 km s^{-1}; additionally, Weedman (1968) finds a positive gradient of V_{PN} with the distance to the center of about 7 km s^{-1} – (arcsec)$^{-1}$. In fact, he registers expansional velocities amounting to 40 km s^{-1} at larger distances from the center (8 arcsec). Here, a value of $V_{PN} \gtrsim 22$ km s^{-1} is adopted.

In this work some of the properties of the suspected halo of NGC 3242 have been studied in an attempt to clarify its nature. Firstly, a search for this halo in the red and blue *POSS* prints has been carried out but only the arc could be seen; one can barely perceive a very faint elliptical nebulosity but it was impossible to be sure it was really there. The arc is barely detectable in the *POSS* red print. This implies that, the Hα surface brightness, S(Hα), should be 5.5×10^{-6} erg cm^{-2} s^{-1} strad^{-1} (Peimbert, Rayo, and Torres-Peimbert 1975) if the contribution of the [N II] lines is negligible but since this contribution is not negligible in the present case (see below) one can correct this contribution by assuming an [N II] (λλ6548, 6584 A)/Hα ratio of about 0.5 and by assuming the same reddening correction as in the PN. The two effects cancel themselves out and one obtains almost the same limiting surface brightness. Since the emission measure, EM (pc cm^{-6}) is related to the unreddened Hα flux in the following form:

$$S(H\alpha) = 8.75 \times 10^{-8}\ EM \qquad (4)$$

(case B photoionized nebula with $T_e = 10^4$ °K), thus EM $\gtrsim$ 60 pc cm^{-6} which implies an rms electron density n_e (rms) $\gtrsim$ 76 or 110 cm^{-3} if an angular diameter of 21 arcmin and a distance of 1.697 or 0.787 kpc are assumed respectively. This estimate is made by assuming implicitly that the existent halo has the dimensions reported by Bond (1981). The electron density of the halo seems to be, at least, a factor of 20 lower than the electron density of the central PN.

Hα and [N II] monochromatic photographs of a field of about 11 arcmin in diameter covering the brightest arc were obtained (see Figure 6, Plate). From these, it can be seen that –contrary to the low [N II]/Hα ratio of the PN itself– the arc has higher [N II]/Hα line-ratios. The Hα photograph reveals two distinct components in this nebulosity: a set of fine filaments, also seen in the [N II] photograph, and a diffuse emission region.

Three FP interferograms of this region were obtained in Hα and [N II]. The radial velocity field obtained from these interferograms is shown in Figure 3. From these data one can obtain the systemic velocities of both the filamentary and the diffuse regions of the arc. The heliocentric values of these velocities are of +15.5±7.9 , +7.7±9.5 km s^{-1} respectively, as compared with the heliocentric velocity of the central PN of 6.3±2 km s^{-1}. Thus, the diffuse component of the arc has the same systemic velocity (within the uncertainties) as that of the central PN, suggesting a physical association between the arc and the PN. On the other hand, the systemic velocity of the filaments is slightly higher. If this difference is significant it may be due to an expansional motion in which case only one half of the expanding shell is seen. The velocity of expansion of the arc would be: $V_a = V_\odot$ (filaments) – $V_\odot$(PN). Given the uncertain-

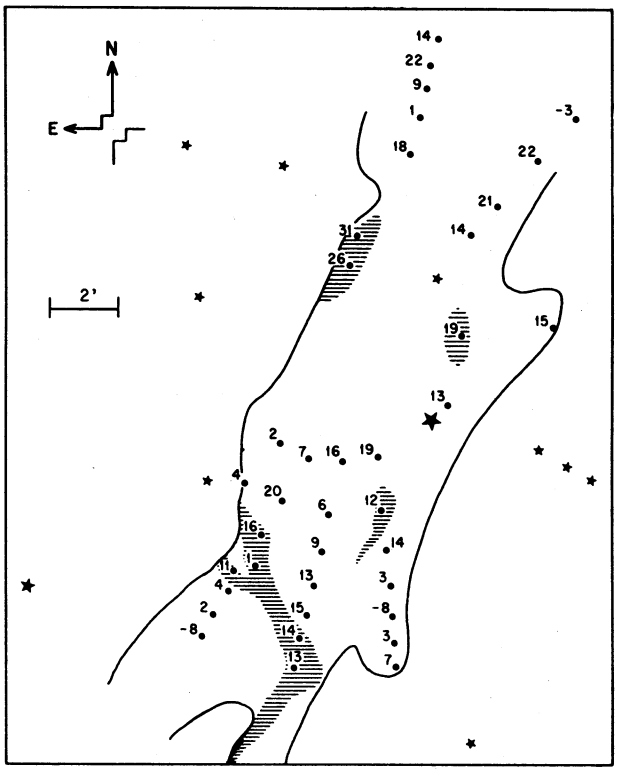

Fig. 3. The heliocentric radial velocity field of the nebulous arc associated with NGC 3242. The hatched area shows the filamentary regions.

ties in the estimation of the systemic velocities shown above it is quite difficult to obtain a more reliable value of V_a; one finds $V_a \cong 9.2 \pm 7.9$ km s^{-1}. If the arc effectively forms part of a larger "halo" surrounding the PN as Bond (1981) has claimed, this estimate of the arc expansional motion may throw light on the mechanism of the halo formation (Jewitt *et al.* 1986). In fact, a comparison between V_a and V_{PN} ($\gtrsim$ 22 km s^{-1}) favors the model of multiple ejection of PN shells or the model of colliding winds of Kwok, Purton, and Fitzgerald (1978). One can note that the predictions of these models remain valid even if the differences in systemic velocities are not significant since there are no other signs of expansional motion of the arc.

On the other hand, by comparing the systemic velocity of the PN with the circular rotational velocity of the neighbouring gas at distances of 0.787 of 1.697 kpc, one obtains that the PN has peculiar velocities of about 17 or 30 km s^{-1} respectively. Further work on this nebulosity is required, in particular a complete mapping of the region in order to detect the whole elliptical nebulosity claimed by Bond (1981).

IV. DISCUSSION

The monochromatic photographs and the kinematical data obtained on G 339.2−0.4 and S 216 favor the classification of these nebulae as PN of large diameter. These nebulae have several common features; both have a diffuse appearance, they do not show violent motions, their spectra indicate low excitation, their densities are lower than those of typical PN, they have a motion which deviates from the circular rotational motion of the surrounding gas and they seem to have faint exciting stars. The inconclusive identification of their exciting stars is the main argument against their identification as PN. It is necessary to study the possible stellar candidates in order to confirm or reject this identification.

On the other hand, it is important to note that the large peculiar velocities of these PN (in particular, that of G 339.2−0.4) could produce changes in the morphology of the nebulae if these peculiar velocities are effectively that large. According with Smith (1976), a decentering of the star relative to the nebula is predicted. This should be confronted with the data and thus serve as an independent method of evaluating the distance to the nebulae. By applying Smith's (1976) model to G 339.2−0.4, by using the parameters deduced in §III*a* and by assuming a neighbouring gas with electron density of 1 cm^{-3}, the predicted decentering of the PNN comes to about 1.2 arcmin. The proposed candidate for the exciting star is effectively decentered by an amount similar to the predicted one.

With respect to the suggested halo of NGC 3242, this work does not corroborate nor reject, the existence of a complete nebulosity around the PN; however, the existence of an arc centered on the PN is an evidence in favor of the existence of the halo. This work gives evidence in favor of a physical connection of the visible arc with the PN. Furthermore, by assuming that this arc forms part of the suggested halo and by taking into account the large uncertainties, it seems that the halo expansion velocity (if any) is lower than that of the PN but this result must be confirmed with more observations. Here again, there appears the possibility of large peculiar velocities of the PN (and its halo) with respect to the surrounding ISM. Although the peculiar velocity may not affect too much the central PN, it could be important in shaping the halo of larger dimensions. However, since the whole shape of the halo is not known with certainty, one must await further observations as suggested in §III*c*.

It is a pleasure to acknowledge the interesting comments of P. Pişmiş and of the anonymous referee. I would also like to thank A. García, E. Themsel, J. Orta, L. Quijada and R. Escamilla for helping in the preparation of the manuscript. This is Contribution No. 190 of Instituto de Astronomía, UNAM.

REFERENCES

Abell, G.O. 1966, *Ap.J.*, **144**, 259.
Aller, L.H. 1976, *Mem. Soc. Roy. Sci. Liège*, **9**, 271.
Barker, T. 1978, *Ap. J.*, **219**, 914.
Bohuski, T.J. and Smith, M.G. 1974, *Ap. J.*, **193**, 197.
Bond, H.E. 1981, *Pub. A.S.P.*, **93**, 429.
Cerruti-Sola, M. and Perinotto, M. 1985, *Ap. J.*, **291**, 237.

Clark, D.H., Caswell, J.L., and Green, A.J. 1975, *Australian J. Phys. (Astrophys. Suppl.)*, **37**, 1.
Courtès, G. 1960, *Ann. d'Ap.*, **28**, 683.
Cudworth, K.M. 1974, *A.J.*, **79**, 1384.
Fesen, R.A., Blair, W.P., and Gull, T.R. 1981, *Ap. J.*, **245**, 131.
Jewitt, D.C., Danielson, G.E., and Kupferman, P.N. 1986, *Ap. J.*, **302**, 727.
Kaftan-Kassim, M.A. 1966, *Ap. J.*, **145**, 658.
Kaler, J.B. 1974, *A.J.*, **79**, 594.
Kaler, J.B. 1981, *Ap. J. (Letters)*, **250**, L31.
Kwok, S., Purton, C.R., and Fitzgerald, M.P. 1978, *Ap. J. (Letters)*, **219**, L125.
Maciel, W.J. and Pottasch, S.R. 1980, *Astr. and Ap.*, **88**, 1.
Marsalkova, P. 1974, *Ap. and Space Sci.*, **27**, 3.
Milne, D.K. and Aller, L.H. 1975, *Astr. and Ap.*, **38**, 183.
Monnet, G. 1970, *Astr. and Ap.*, **9**, 420.
Murdin, P., Clark, D.H., and Havnes, R.F. 1979, *M.N.R.A.S.*, **189**, 459.
Osterbrock, D.E. 1974, in *Astrophysics of Gaseous Nebulae*, eds. G. Burbidge and M. Burbidge (San Francisco: Freeman and Co.).
Parker, R.A.R., Gull, T.R., and Kirshner, R.P. 1979, *An Emission Line Survey of the Milky Way*, NASA SP-434.
Peimbert, M., Rayo, J.F., and Torres-Peimbert, S. 1975, *Rev. Mexicana Astron. Astrof.*, **1**, 289.
Pradhan, A.K. 1978, *M.N.R.A.S.*, **193**, 89p.
Reynolds, R.J. 1985, *Ap. J.*, **288**, 622.
Rosado, M. 1983, *Rev. Mexicana Astron. Astrof.*, **8**, 59.
Rosado, M., and Kwitter, K.B. 1982, *Rev. Mexicana Astron. Astrof.*, **5**, 217.
Rosado, M., Georgelin, Y.M., Georgelin, Y.P., Laval, A., and Monnet, G. 1982, *Astr. and Ap.*, **115**, 61.
Sabbadin, F. and Minello, S. 1978, *Astr. and Ap. Suppl.*, **33**, 223.
Shönberner, D. 1981, *Astr. and Ap.*, **103**, 119.
Smith, H. 1976, *M.N.R.A.S.*, **175**, 419.
van den Bergh, S. 1978, *Ap. J. Suppl.*, 38, 119.
Weedman, D.W. 1968, *Ap. J.*, **153**, 49.
Weinberger, R., Dengel, J., Hartl, H., and Sabbadin, F. 1983. *Ap. J.*, **265**, 249.
Welty, D.E. 1983, *Pub. A.S.P.*, **95**, 217.
Wilson, O.C. 1950, *Ap. J.*, **111**, 279.
Zealey, W.J., Elliot, K.H., and Malin, D.F. 1979, *Astr. and Ap. Suppl.*, **38**, 39.

Margarita Rosado: Instituto de Astronomía, Apartado Postal 70-264, 04510 México, D.F., México.

Rev. Mexicana Astron. Astrof., 13, 57-64 (1986)

CORRELATIONS BETWEEN OBSERVATIONAL PARAMETERS OF THE CONDENSATIONS IN HERBIG–HARO OBJECT 2

J. Cantó and L.F. Rodríguez

Instituto de Astronomía
Universidad Nacional Autónoma de México

Received 1986 February 26

RESUMEN

En este trabajo se presentan correlaciones observacionales entre la intensidad de la línea Hα y la densidad electrónica deducida de las líneas rojas de [S II], con la velocidad espacial en las partes más brillantes de las condensaciones de HH2. Se muestra también, que existe una correlación entre el tamaño de la condensación y su velocidad. Estas correlaciones son en el sentido: intensidad de Hα $\propto V^2$; densidad electrónica $\propto V$ y tamaño $\propto V$. Las primeras dos correlaciones se pueden explicar bajo un modelo en el cual, la parte más brillante de cada condensación representa una onda de choque plano–paralela moviéndose con una velocidad igual a la velocidad observada de la condensación: todas las ondas moviéndose en el mismo medio. Estas ondas de choque planas se interpretan como las cabezas de las ondas de choque en forma de arco que se forman cuando condensaciones de alta velocidad se mueven en el medio interestelar. La última de las correlaciones podría también explicarse con el mismo modelo, puesto que la zona emisora de una onda de choque en forma de arco (para un tamaño de condensación fijo) aumenta linealmente con la velocidad de la onda.

ABSTRACT

In this paper we present empirical correlations between the Hα line intensity and [S II] electron density with the total spatial velocity for the brightest part of individual knots in HH2. Also we show that there is a correlation between the size of a knot and its total velocity. These correlations are in the sense: Hα intensity $\propto V^2$; electron density $\propto V$ and size $\propto V$. The first two correlations fit with a model in which the brightest part of each knot represents a single plane-parallel shock wave with velocity equal to the spatial velocity of the knot, all moving into the same medium. These plane-parallel shocks are interpreted as the heads of bow shocks formed as high-velocity clumps plunge into the interstellar medium. The last correlation may also be explained since the extent of the emitting zone of a bow shock (for a given clump size) increases linearly with velocity.

Key words: HERBIG-HARO OBJECTS — SHOCK WAVES

I. INTRODUCTION

Since the time of their discovery by Haro (1950) and Herbig (1951), one of the most important aspects of the Herbig-Haro object phenomenon has been their excitation mechanism. The pioneering work of Böhm (1956), Osterbrock (1958) and Haro and Minkowski (1960) firmly established that HH-objects could not be the result of simple photoionization from a central source. In 1975, Schwartz (1975) drew attention to the great similarities between the optical spectra of these objects and the SNR N49 in the LMC. This fact pointed to the interpretation of HH-objects as the cooling region of interstellar shock waves of moderate velocity. Fitting with this interpretation there were the highly supersonic radial velocities exhibited by most objects. Years later, Raymond (1976, 1979), Dopita (1978) and Shull and McKee (1979) performed detailed calculations of the emission spectra of plane-parallel shock waves in steady state and showed that the mean observed features in the optical spectra of HH-objects could be reproduced with preshock densities of ~ 100 cm^{-3} and shock velocities of ~ 100 km s^{-1}.

A real challenge for the interpretation of HH-objects as simple (plane-parallel and steady state) shock waves came with the detection of ultraviolet emission from these objects (see Böhm 1983 and references therein). The *UV* spectra of HH1 and 2 show emission lines of highly ionized ions (C III and IV, O III and IV and Si III and IV) whose strength can not be reproduced with the same shock model which accounts for the optical spectra. A much larger (~ 200 km s^{-1}) shock velocity is suggested from the high excitation *UV* emission lines. A plausible explanation for this apparent disagreement is that HH-objects represent bow shocks which are the result of the interaction of dense clumps of material against a less dense supersonic stream (Schwartz 1978; Hartmann and Raymond 1984). In this case, the ob-

served spectrum would be the blend of the spectra of a continuum of shocks with velocities ranging from the velocity of the impinging stream (the maximum velocity) down to zero. Further evidence for a bow geometry in HH-objects is given by the fact that the predicted line shapes are similar to those observed (Choe, Böhm, and Solf 1984).

Hartmann and Raymond (1984) have presented detailed calculations of the spectra of bow shocks with maximum velocities in the range 160-300 km s^{-1}. They found that the line widths and the optical and *UV* spectra of HH1 and HH2 are in reasonable agreement with calculations for maximum shock velocities of $\sim$ 200 km s^{-1}. Since such velocities are comparable to the spatial (radial plus transverse) velocities of the knots in HH1 and HH2, it was concluded that HH-objects represent high velocity dense clumps shocking with less dense interstellar material.

In this paper we present further evidence in this sense. Our study is restricted to HH2 for which spectroscopic, radial and proper motion information for individual condensations is available. In §II we discuss the data and present the correlations between the electron density, Hα line intensity and size of condensations with their spatial velocity. In §III we interpret these correlations in the framework of the shock wave theory, while in §IV we give our conclusions.

II. DISCUSSION OF THE DATA

Most of the spectrophotometric observations of HH-objects available in the literature have been performed in such a way that the slit or the diaphragm used included entire objects or entire knots within one object. The spectra obtained in this way are then likely to correspond to the entire bow shock, and thus their interpretation in terms of simple plane-parallel, steady state shock waves is inadequate. They should be interpreted in terms of bow shock models (Hartmann and Raymond 1984).

In contrast, the study by Schwartz (1978) of individual knots in HH2 was done using a slit of only 1″, which is substantially smaller than the apparent size of knots in this object. Also, the length and width of the PDS slit was chosen in such a way that it was much less than the length of a given emission knot on the plate. Furthermore, traces were made parallel to the dispersion through the central portion of each line. These three facts suggest that the emission line intensities reported by Schwartz correspond (mainly) to the central, brightest parts of each knot, that is, that they correspond to the central parts of the bow shocks. In this case, we expect the line spectra to be easier to interpret, since the central part of a bow shock can roughly be approximated as plane-parallel. The velocity of the shock is the velocity of the impinging stream.

Having this idea in mind, we adopt the relative line intensities reported by Schwartz (1978) as our basic set of data. In Table 1 we give the intensity of the Hα line (in arbitrary units) and the electron density dependent intensity ratio of the [S II] red lines. Also we list in this table the corresponding electron densities for $T = 10^4$ K.

First we investigate if there is any correlation between the Hα intensity and the electron density with the total (spatial) velocity of the knots. For this, we use the radial velocities also reported by Schwartz (1978) and the tan-

TABLE 1

OBSERVED AND DERIVED PARAMETERS FOR INDIVIDUAL KNOTS IN HH2

Condensation	V_r[1] (km s^{-1})	ΔV_r[2] (km s^{-1})	ΔV_T[3] (km s^{-1})	V_{TOT}[5] (km s^{-1})	I (6717)/I(6731)[6]	log n_e[8] (cm^{-3})	I (Hα)[10]	D[11] (arcsec)
A	21 ± 4	3 ± 4	153:[4]	153:	0.67	3.26 ± 0.17	141	3.3 ± 0.3
B	13 ± 6	− 5 ± 6	100 ± 13	100 ± 13	0.72	3.14 ± 0.15	112	2.0 ± 0.1
C	31 ± 5	13 ± 5	294 ± 24	294 ± 24	0.96[7]	2.70 ± 0.18[9]	64	1.3 ± 0.1
D	...	...	85 ± 22	...	...	...	...	1.4 ± 0.2
E	39 ± 6	21 ± 6	61 ± 22	65 ± 22	0.77	3.04 ± 0.15	52	1.6 ± 0.2
G	− 2 ± 8	− 20 ± 8	153 ± 9	154 ± 9	0.62	3.40 ± 0.16	285	2.8 ± 0.2
H	13 ± 2	− 5 ± 2	241 ± 13	241 ± 13	0.53	3.66 ± 0.18	652	4.4 ± 0.2
I	...	...	?38 ± 48	...	...	...	...	1.0 ± 0.1
L	11 ± 3	− 7 ± 3	...	...	0.77	3.76 ± 0.18	26	1.6 ± 0.2

1. Heliocentric radial velocity derived from the red lines of [O I], [N II], Hα and [S II] (Schwartz 1978).
2. Radial velocity with respect to the cloud; $\Delta V_r = V_r$ (HH) − V_r (cloud); V_r (cloud) = + 18 km s^{-1} (Schwartz 1978).
3. Tangential velocity with respect to the cloud (Herbig and Jones 1981). Adopted distance 460 pc.
4. In the late 1950's a new nucleus (A') appears about 1″ north of A. This new nucleus has a tangential velocity of 46.5 km s^{-1}
5. Total spatial velocity with respect to the cloud; $V_{TOT} = (\Delta V_r^2 + \Delta V_T^2)^{1/2}$.
6. Ratio of relative intensities obtained through a 1″ slit and uncorrected for extinction (Schwartz 1978).
7. Relative intensities between lines in a given knot are in agreement ($\sim$ 20%) with data reported by other authors (Dopita 1978; Böhm, Siegmund and Schwartz 1976). However for this condensation Dopita (1978) reports $\sim$ 0.50.
8. Electron density derived from the [S II] ratio for $T = 10^4$ K, using the transition probabilities of Mendoza and Zeippen (1982) and the reaction-rate parameters of Pradhan (1978).
9. For the ratio 0.5 given by Dopita (1978), log $n_e = 3.76 \pm 0.18$.
10. Relative intensities obtained through a 1″ slit and uncorrected for extinction in arbitrary units (Schwartz 1978).
11. Angular diameter estimated from the 1980 (Figure 2) of Herbig and Jones (1981). Errors are derived from three independent measurements.

gential velocities corresponding to the proper motions measured by Herbig and Jones (1981). We adopt a distance of 460 pc. The velocities of each knot are also given in Table 1.

Figure 1*a* is a plot of the Hα line intensities and the [S II] electron densities of each knot against their spatial velocities. Clearly both quantities are *directly* correlated with velocity. The electron density increases with velocity, approximately as $\propto V$; while the Hα line intensity increases with velocity as $\propto V^2$. These correlations will be discussed in the next section. Here we just point out that these correlations are *opposite* to the correlations that Schwartz and Dopita (1980) propose to exist among a large sample of HH-objects. These authors present plots of the modulus of the radial velocity and the excitation state within the object (estimated by the ratio [O III] λ5007/[O I] λ6300) against the modulus of the radial velocity and the [S II] electron density. In their view, the lack of HH-objects with high radial velocities showing high excitation or having high electron density indicates that the velocity of the shock wave and the velocity of the emitting material are *inversely* related. As we will see in the next section, this conclusion is exactly the opposite to that indicated by Figure 1.

Another empirical correlation which is likely to give us information on the origin of HH-objects is that shown in Figure 2. There, we plot the apparent angular size of each condensation (estimated from the 1980 photograph of Herbig and Jones (1981); their Figure 2) against its spatial velocity. Again it appears to be a direct correlation between them, *vis.*, (angular size) $\propto V$. This correlation will also be discussed in the next section.

III. DISCUSSION OF THE MODEL

As we will see the correlations between the Hα line intensity and the [S II] electron density with the total (spatial) velocity of the condensations can be understood in a model in which each condensation of HH2

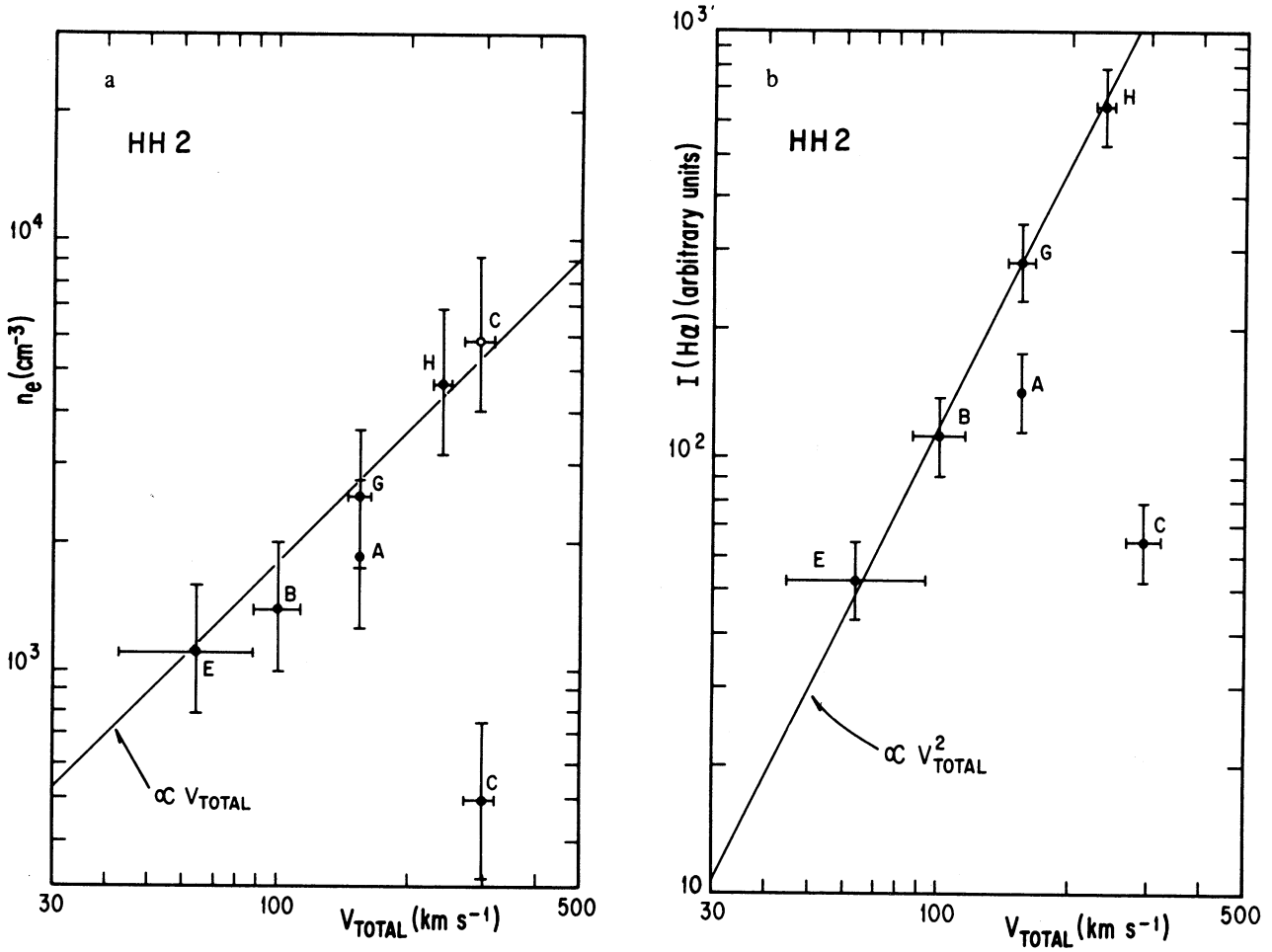

Fig. 1. Correlations between (a) electron density, and (b) Hα line intensity with their spatial velocity for the brightest parts of individual condensations in HH2. The data and the sources of information are given in Table 1. The open circle in (a) represents the measurement of Dopita (1978).

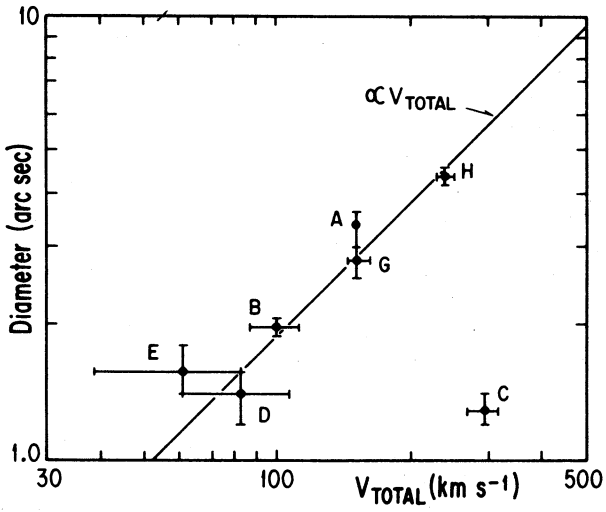

Fig. 2. Correlation between the angular diameter of condensations in HH2 with their spatial velocity. The broken line represents the predicted behaviour (Rozyczka and Tenorio-Tagle 1985) if the condensations represents bow shocks produced by clumps of similar sizes but different velocities.

(actually its brightest part) represents a single plane-parallel steady shock wave moving with a velocity equal to its spatial velocity. All condensations are moving in the same medium.

In Appendix I we consider a strong, plane-parallel, steady state shock wave moving with velocity v_0 into a medium with hydrogen density n_0, thermal pressure P_0 and magnetic field intensity B_0 parallel to the shock front. There, we show that the electron density that would be deduced from the [S II] line ratio in the case of a non-negligible magnetic field is,

$$\left[\frac{n_e}{\text{cm}^{-3}}\right] = 3.82 \times 10^3 \left[\frac{n_0}{100\ \text{cm}^{-3}}\right]^{3/2} \left[\frac{B_0}{10\ \mu\text{G}}\right]^{-1} \left[\frac{v_0}{100\ \text{km s}^{-1}}\right] \quad (1)$$

We notice that Eq. (1) gives a linear dependence on the shock velocity. Recalling that the observed dependence of the electron density with the total velocity for condensations in HH2 is also linear, it is natural to propose a model in which the brightest part of each condensation represents a single plane-parallel, steady shock, with velocity equal to the spatial velocity of the condensation and all moving into a same medium with a non-negligible magnetic field.

This model can be tested by comparing the observed correlation between the intensity of the Hα line and velocity ($\propto V^2$; § II) with that predicted by the model. For this we use the detailed calculations of the emission by plane-parallel, steady state shock waves by Raymond (1976, 1979) and Shull and McKee (1979). Figure 3 shows the Hα line intensity (erg cm^{-2} s^{-1} str^{-1}) as a function of the shock velocity for several models with the same $n_0 = 10$ cm^{-3}, $B_0 = 1\mu$G and abundances (cosmical), as given by Raymond (1976) and Shull and Mc Kee (1979). The two sets of models show an increase of the Hα line intensity with velocity approximately as $\propto V^2$ (except for $V \lesssim 70$ km s^{-1} in Shull and McKee's models). Indeed, the straight line on Figure 3 represents a fit to Raymond's models of the form

$$\left[\frac{I(\text{H}\alpha)}{\text{erg cm}^{-2}\ \text{s}^{-1}\ \text{str}^{-1}}\right] = 1.66 \times 10^{-9} \left[\frac{V_s}{\text{km s}^{-1}}\right]^2 \quad (2)$$

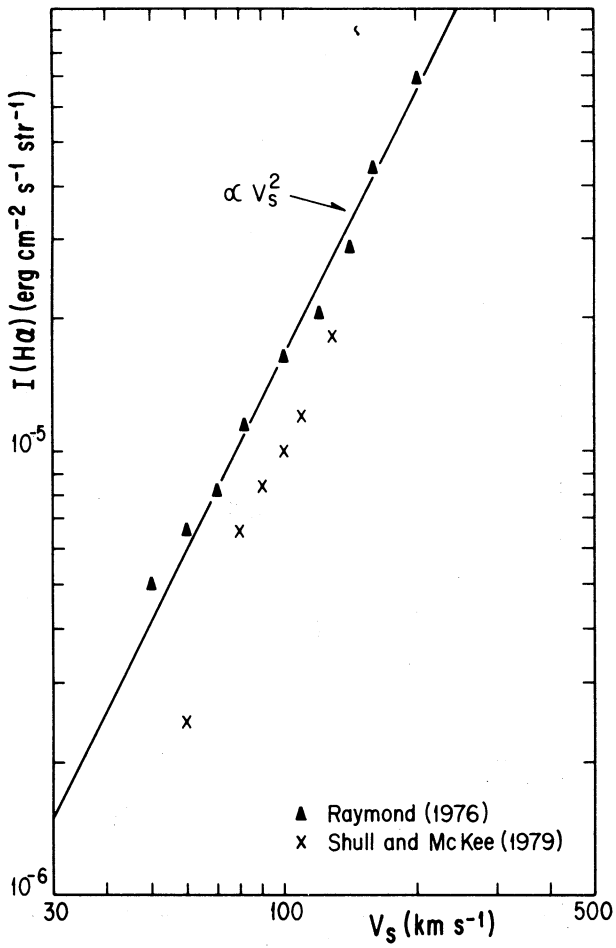

Fig. 3. Hα line intensity predicted by shock models as a function of shock velocity. The pre-shock hydrogen density and magnetic field strength are 10 cm^{-3} and 1 μG, respectively, for all models. The line represents a fit to Raymond's models.

A similar fit can be obtained for Shull and McKee's models for shock velocities $V \gtrsim 70$ km s^{-1}, although the scale coefficient is ~ 1.6 times lower than the value given in Eq. (2). The differences in the scale factor and in the behavior of the Hα intensity for $V \lesssim 70$ km s^{-1} between the two sets of models is likely to be the result of different assumptions regarding the pre-shock ionization. Raymond assumes complete pre-ionization of hydrogen, while Shull and McKee calculate it in a self-consistent manner by considering the flux of ionizing photons produced in the wave and travelling upstream.

In any case, it appears that in the range of velocities considered in this work, the Hα line intensity is expected to increase as the square of the shock velocity. This is the same behavior we observe in the condensations of HH2 (Figure 1*b*), if we identify the spatial velocity of each condensation with the velocity of the shock that gives rise to the Hα emission. Thus, our model of individual shock waves moving with a velocity equal to the spatial velocity of the emitting material is further supported.

Adopting this model we now proceed to estimate the parameters (n_0 and B_0) of the pre-shock medium. For this, we first compare Eq. (1) with the fit in the $n_e - V_{TOT}$ plot of Figure 1*a*.

$$\left[\frac{n_e}{\text{cm}^{-3}}\right] = 1.78 \times 10^3 \left[\frac{V_{TOT}}{100 \text{ km s}^{-1}}\right]$$

to obtain

$$\left[\frac{n_0}{100 \text{ cm}^{-3}}\right]^{3/2} \left[\frac{B_0}{10\,\mu\text{G}}\right]^{-1} = 0.47 \qquad (3)$$

where we have identified the total velocity of the knots with the shock velocity.

This result can be combined with the absolute fluxes of the Hα line for individual condensations in HH2 and the shock models to estimate n_0 and B_0 separately. According to Brugel, Böhm, and Mannery (1981), the absolute flux in the Hα line above the Earth's atmosphere corrected for extinction for condensation H of HH2 is $\sim 8.7 \times 10^{-13}$ erg cm^{-2} s^{-1}. Adopting for this condensation an angular diameter of 4.4″ (Table 1), an intensity of $\sim 2.5 \times 10^{-3}$ erg cm^{-2} s^{-1} str^{-1} in this line is derived.

As we showed above (see also Raymond 1976), the detailed shock calculations indicate $I(H\alpha) \propto V_s^2$. Also, from these calculations we found that I(Hα) seems to be directly proportional to the pre-shock density, n_0, and nearly insensitive to B_0. The models presented in Figure 3 were calculated with $n_0 = 10$ cm^{-3}. Thus the Hα line intensity as a function of n_0 and V_s may be written as

$$\left[\frac{I(H\alpha)}{\text{erg cm}^{-2}\text{ s}^{-1}\text{ str}^{-1}}\right] \cong 1.66 \times 10^{-8} \left[\frac{n_0}{100 \text{ cm}^{-3}}\right] \left[\frac{V_s}{\text{km s}^{-1}}\right]^2 \qquad (4)$$

where we have used Eq. (2). Taking for HH2-H, $V_s \cong 240$ km s^{-1} (the total spatial velocity; Table 1) and $I(H\alpha) \cong 2.5 \times 10^{-3}$ erg cm^{-2} s^{-1} str^{-1} (see above), Eq. (4) gives,

$$n_0 \cong 260 \text{ cm}^{-3}$$

a reasonable value for the outer parts of molecular clouds.

Using this estimate for the pre-shock hydrogen density in Eq. (3), one finds,

$$B_0 \cong 89\ \mu\text{G}$$

as a rough estimate. We can see, however, that this estimate for the pre-shock magnetic field is consistent with the limits we derive from the relation, given by Brown and Chong-An Chang (1983), between the magnetic field strength and the gas density in interstellar clouds, *vis.*,

$$\left[\frac{B}{\mu\text{G}}\right] = 3.8^{+17}_{-3.1} \left[\frac{n}{\text{cm}^{-3}}\right]^{0.44}$$

when it is extrapoled to dense molecular clouds. For $n \sim 260$ cm^{-3} we obtain $B = 0.8 - 240\ \mu$G.

Finally, we will discuss the correlations between the diameter of the knots and their spatial velocity (Figure 2). The solid line in Figure 2 represents the fit,

$$\left[\frac{d}{\text{arcsec}}\right] = 1.91 \times 10^{-2} \left[\frac{V_{TOT}}{\text{km s}^{-1}}\right] \qquad (5)$$

This correlation may also be explained in a model in which each condensation represents a bow shock, all moving into the same medium. Rozyczka and Tenorio-Tagle (1985) have recently investigated the properties of bow shocks which are formed around dense clumps impinged by a supersonic stream. In particular, they show (their Figure 4) maps of the total (frequency-integrated) emission of the shock for velocities in the range 25–400 km s^{-1}. For velocities between 25 and 200 km s^{-1}, it is found that the bulk of the optical

emission comes from the head of the bow shock, with the emission dropping very rapidly towards the lee side of the clump. The extent of the emitting zone perpendicular to the flow direction is always similar to the clump radius and does not change appreciably with velocity. The length (measured along the flow direction), however, is an increasing function of velocity. It is clear that the predicted behaviour is quite similar to that observed, if each condensation represents a bow shock produced by clumps of similar size but moving at different velocities.

Nevertheless, there is a problem with this interpretation of the empirical behaviour. The condensations in HH2 are approximately round, while the Rozyczka and Tenorio-Tagle (1985) modeling would imply emitting zones elongated along the direction of motion. We conclude that this last correlation (diameter $\propto$ spatial velocities) can be accounted for only partially.

IV. CONCLUSIONS

Our main conclusions can be summarized as follows:

1) The Hα line intensity and [S II] electron density from the central brightest part of individual knots in HH2 show direct correlations with their total spatial velocity. The size for individual knots also increases with the total velocity. More specifically:

a) Hα line intensity $\propto V_{TOTAL}^2$
b) Electron density $\propto V_{TOTAL}$
c) Angular diameter $\propto V_{TOTAL}$.

2) Correlations (a) and (b) can be interpreted in a model in which the brightest part of each condensation represents a single, plane-parallel shock wave with velocity equal to the total spatial velocity of the condensation. These plane-parallel shocks are interpreted as the heads of bow shocks formed as high-velocity clumps plunge into the interstellar medium.

3) The estimated values for the hydrogen density and magnetic field of the medium through which the clumps are moving at ~ 260 cm^{-3} and ~ 90 μG respectively. These values are consistent with those expected to prevail in the outer parts of molecular clouds.

4) Correlation (c) may be explained partially in terms of bow shocks if the clumps have similar sizes but are moving at different velocities.

5) These results suggest that, at least for HH2, we can favor the model of the "interstellar bullets" (dense clumps moving supersonically in a tenuous ambient medium, Norman and Silk 1979; Rodríguez *et al.* 1980) as opposed to the model of "cloudlets" being shocked by a stellar wind (Schwartz 1978). However, for other HH objects the results of Schwartz and Dopita (1980) favor the "cloudlet" model. It is obvious that further research is needed before this basic characteristic of the kinematics of HH objects can be determined.

This work was partially supported by a grant from *CONACYT* (México), No. PCCBBNA-022688. This is Contribution No. 194 of Instituto de Astronomía, UNAM.

REFERENCES

Böhm, K.H. 1956, *Ap. J.*, **123**, 379.
Böhm, K.H. 1983, *Rev. Mexicana Astron. Astrof.*, **7**, 55.
Böhm, K.H., Siegmund, W.A., and Schwartz, R.D. 1976, *Ap. J.*, **203**, 399.
Brown, R.L. and Chong-An Chang, 1983, *Ap. J.*, **264**, 134.
Brugel, E.W., Böhm, K.H. and Mannery, E. 1981, *Ap. J. Suppl.*, **47**, 117.
Choe, S.U., Böhm, K.H., and Solf, J. 1984, *Ap. J.*, **288**, 338.
Dopita, M.A. 1978, *Ap. J. Suppl.*, **37**, 117.
Haro, G. 1950, *Ap. J.*, **55**, 72.
Haro, G. and Minkowski, R. 1960, *Ap. J.*, **65**, 490.
Hartmann, L. and Raymond, J.C. 1984, *Ap. J.*, **276**, 560.
Herbig, G.H. 1951, *Ap. J.*, **113**, 697.
Herbig, G.H. and Jones, B.F. 1981, *A.J.*, **86**, 1232.
Mendoza, C. and Zeippen, C.J. 1982, *M.N.R.A.S.*, **199**, 1025.
Norman, C. and Silk, J. 1979, *Ap. J.*, **228**, 197.
Osterbrock, D.E. 1958, *P.A.S.P.*, **70**, 399.
Pradhan, A.K. 1978, *M.N.R.A.S.*, **183**, 89p.
Raymond, J.C. 1976, Ph.D. Thesis, University of Wisconsin Madison.
Raymond, J.C. 1979, *Ap. J. Suppl.*, **39**, 1.
Rodríguez, L.F., Moran, J.M., Ho, P.T.P., and Gottlieb, E.W. 1980, *Ap. J.*, **235**, 845.
Rozyczka, M. and Tenorio-Tagle, G. 1985, *Astr. and Ap.*, **147**, 220.
Schwartz, R.D. 1975, *Ap. J.*, **195**, 631.
Schwartz, R.D. 1978, *Ap. J.*, **223**, 884.
Schwartz, R.D. and Dopita, M. 1980, *Ap. J.*, **236**, 543.
Shull, J.M. and McKee, C.F. 1979, *Ap. J.*, **220**, 525.

APPENDIX I

ELECTRON DENSITY–SHOCK VELOCITY RELATION IN ISOTHERMAL SHOCKS

Consider a plane-parallel steady flow with mass density ρ_0, thermal pressure P_0, magnetic field B_0 perpendicular to the flow, and velocity v_0 with respect to the shock front. Conservation of mass and momentum gives,

$$\rho v = \rho_0 v_0 \qquad \text{(A1)}$$

$$P + \rho v^2 + \frac{B^2}{8\pi} = P_0 + \rho_0 v_0^2 + \frac{B_0^2}{8\pi} \qquad \text{(A2)}$$

where P, ρ, v and B are the values of the variables at any point in the relaxation region behind the shock front. If the magnetic field is assumed to be frozen-in, then,

$$\frac{B}{\rho} = \frac{B_0}{\rho_0} \quad . \qquad \text{(A3)}$$

The pressure and mass density are related by $P = \rho c^2$; where c is the sound speed.

Let us consider that region behind the shock where the temperature has reached its pre-shock value. There, $c = c_0$ and the substitution of (A1) and (A3) in (A2) gives,

$$\frac{1}{2}v_{A_0}^2\left[\left(\frac{\rho}{\rho_0}\right)^2 - 1\right] + c_0^2\left[\left(\frac{\rho}{\rho_0}\right) - 1\right] - v_0^2\left[\frac{(\rho/\rho_0) - 1}{(\rho/\rho_0)}\right] = 0 \qquad \text{(A4)}$$

where $v_{A_0} \equiv (B_0^2/4\pi\rho_0)^{1/2}$ is the Alfvén speed in the unshocked stream. Since we expect $(\rho/\rho_0) \neq 1$, then Eq. (A4) simplifies to

$$\frac{1}{2}v_{A_0}^2\left(\frac{\rho}{\rho_0}\right)^2 + \left[\frac{1}{2}v_{A_0}^2 + c_0^2\right]\left(\frac{\rho}{\rho_0}\right) - v_0^2 = 0 \qquad \text{(A5)}$$

whose solution is,

$$\left(\frac{\rho}{\rho_0}\right) = \sqrt{\left(\frac{1}{2} + \frac{c_0^2}{v_{A_0}^2}\right)^2 + 2\left(\frac{v_0^2}{v_{A_0}^2}\right)} - \left(\frac{1}{2} + \frac{c_0^2}{v_{A_0}^2}\right). \qquad \text{(A6)}$$

Two limiting cases follow. For a negligible magnetic field or a small compression factor (ρ/ρ_0), Eq. (A6) reduces to the familiar result,

$$\left(\frac{\rho}{\rho_0}\right) \cong \left(\frac{v_0}{c_0}\right)^2 \qquad \text{(A7)}$$

which indicates that the compression across an isothermal shock increases as the square of the velocity of the shock.

On the other hand, for a non-negligible magnetic field and/or a strong compression factor, Eq. (A6) yields,

$$\left(\frac{\rho}{\rho_0}\right) \cong 2^{1/2}\left(\frac{v_0}{v_{A_0}}\right) \qquad \text{(A8)}$$

which predicts a linear increase of the compression with the shock velocity.

The critical value for the compression factor (for given pre-shock magnetic field and density) which separates the two regimes can be estimated by the condition,

$$\frac{1}{2}v_{A_0}^2\left(\frac{\rho}{\rho_0}\right)^2 \cong \left(\frac{1}{2}v_{A_0}^2 + c_0^2\right)\frac{\rho}{\rho_0}$$

which yields,

$$\left(\frac{\rho}{\rho_0}\right) \cong 1 + 2\left(\frac{c_0}{v_{A_0}}\right)^2. \qquad \text{(A9)}$$

This compression factor corresponds to a shock velocity

$$v_0 \cong v_{A_0}\left[1 + 2\left(\frac{c_0}{v_{A_0}}\right)^2\right]. \qquad \text{(A10)}$$

Numerically, the pre-shock Alfvén and sound speeds are given by,

$$\frac{v_{A_0}}{\text{km s}^{-1}} = 1.85\left(\frac{B_0}{10\,\mu\text{G}}\right)\left(\frac{n_0}{100\,\text{cm}^{-3}}\right)^{-1/2} \qquad \text{(A11)}$$

and

$$\left(\frac{c_0}{\text{km s}^{-1}}\right) = 7.68\left(\frac{T_0}{10^4\text{K}}\right)^{1/2}(1.1 + \xi_0)^{1/2}$$

where T_0 and n_0 denote the pre-shock temperature and density of hydrogen nuclei, respectively. $\xi_0 (\equiv n_{e_0}/n_0)$ is the pre-shock hydrogen ionization (helium is assumed to remain neutral). A helium to hydrogen particle ratio of 0.1 has been assumed.

Before we proceed to estimate the electron density in the post-shock region, we should mention that Eq. (A6) and thus all the results and conclusions derived from it are also approximately correct for strong shocks even if the isothermal condition is not met. That is, Eq. (A6) gives the density of mass in that part of the cooling region where the temperature equals the pre-shock temperature. However, Eq. (A6) can also be used to estimate the mass density at any point in the cooling region, provided we substitute the pre-shock sound speed c_0 by the sound speed of the region under consideration.

Let n_e and ξ be the electron density and hydrogen ionization ratio in the post-shock region. If helium is also assumed to be neutral in this region,

$$\left(\frac{\rho}{\rho_0}\right) = \frac{n_e}{n_0\xi}$$

and, from Eq. (A6),

$$n_e = \xi n_0 \left[\sqrt{\left(\frac{1}{2} + \frac{c_0^2}{v_{A_0}^2}\right)^2 + 2\left(\frac{v_0}{v_{A_0}}\right)^2} - \left(\frac{1}{2} + \frac{c_0^2}{v_{A_0}^2}\right)^2 \right] \qquad \text{(A12)}$$

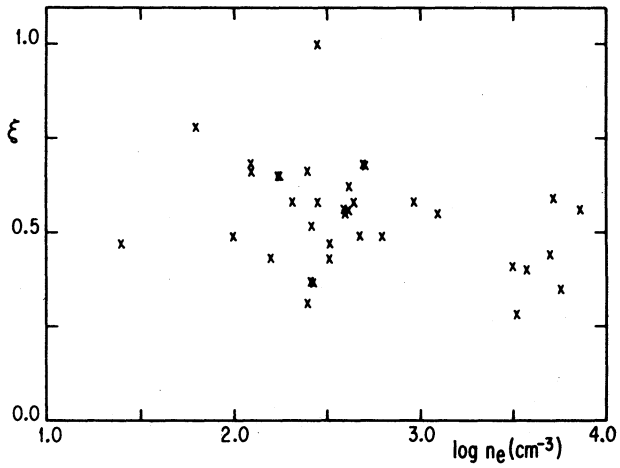

Fig. A1. Hydrogen ionization ratio required by Eq. (A12) to match the electron density deduced from the [S II] lines for each model given by Raymond (1976). Notice that despite the very different shock parameters assumed for each model, the ionization ratio can be taken ~ 0.5, within a factor of two.

in the region where the shocked flow has cooled down to a temperature equal to the pre-shock temperature.

The hydrogen ionization ratio in this region can be estimated by comparing Eq. (A12) with the results of the detailed calculations of the structure of shock waves as reported by Raymond (1976). For this, we use the forbidden red lines of [S II] whose ratio is sensitive to the electron density. The [S II] lines are expected to be emitted mainly in that part of the cooling region where $T \sim 10^4$ K. Figure (A1) shows a plot of the hydrogen ionization ratio required by Eq. (A12) to match the electron density deduced from the [S II] lines for each model given by Raymond (1976). It follows from this figure that Eq. (A12) with $\xi = 0.5$ is able to reproduce Raymond's results within a factor of two.

Finally, we give the numerical expression for the electron density that would be deduced from the [S II] lines ratio in the limiting case of a non-negligible magnetic field and/or a strong compression factor (Eq. (A8)). This is,

$$\left(\frac{n_e}{\text{cm}^{-3}}\right) = 3.82 \times 10^3 \left(\frac{n_0}{100\ \text{cm}^{-3}}\right)^{3/2} \left(\frac{B_0}{10\ \mu\text{G}}\right)^{-1} \left(\frac{V_0}{100\ \text{km s}^{-1}}\right) \qquad \text{(A13)}$$

where we have adopted $\xi = 0.5$.

Jorge Cantó and Luis F. Rodríguez: Instituto de Astronomía, UNAM, Apartado Postal 70-264, 04510 México, D.F., México.

Rev. Mexicana Astron. Astrof., 13, 65-68 (1986)

ABSOLUTE SPECTROPHOTOMETRY OF SEYFERT GALAXIES. (Research Note)

D. Dultzin-Hacyan and M.A. Herrera
Instituto de Astronomía
Universidad Nacional Autónoma de México

N. Núñez
Facultad de Ciencias
Universidad Nacional Autónoma de México

Received 1985 May 2

RESUMEN

Se reportan los resultados de espectrofotometría absoluta para cuatro galaxias Seyfert. Se dan intensidades y anchos equivalentes de algunas líneas no reportadas previamente en la literatura. Se analizan las peculiaridades de cada objeto, tanto en el continuo como en las líneas de emisión, luego de comparar con observaciones anteriores. El comportamiento de Hβ en 3C120 es muy peculiar.

ABSTRACT

The results of absolute spectrophotometry for four Seyfert galaxies are reported. Absolute intensities and equivalent widths are given for several lines not reported before in the literature. Comments on each object's continuum and line spectra are given after comparison with previous observations. The behaviour of Hβ in 3C120 is very peculiar.

Key words: GALAXIES-SEYFERT — SPECTROPHOTOMETRY

I. INTRODUCTION

The recent theoretical studies of Capriotti, Foltz, and Peterson (1982); Blandford and McKee (1982); and Antokhin and Bochkarev (1984) emphasize the importance of the study of the temporal behaviour of the broad-line profiles in Seyfert 1 galaxies as a diagnostic of the structure and dynamics of the broad-line emitting gas.

Although optical-wavelength continuum variability of Seyfert galaxy nuclei has been recognized for at least 15 years (Pacholczyk and Weymann 1968) only within the past few years has it become clear that the broad emission line spectra of Seyfert 1 galaxies change in response to changes in the continuum flux. Consequently, systematic monitoring of the continuum flux and line profiles is potentially a valuable diagnostic of conditions within the Broad Line Region (BLR).

It is important that such observations be carried out in a consistent fashion: with the same instruments and under similar observing conditions. A few galaxies have been observed in this way (see e.g. Alloin *et al.* 1985). Unfortunately, this is not always possible, and the 'second best' alternative is to compare one's observations with those found in the literature, provided that due attention is paid to the effects of different observational conditions (see e.g. Peterson *et al.* 1982, 1984).

II. OBSERVATIONS

The observations were carried out during two seasons: August 1981 and October 1982 with the 2.1-m telescope of the Observatorio Astronómico Nacional at San Pedro Mártir, Baja California, using a low dispersion Boller and Chivens spectrograph coupled with the Optical Multichannel Analyzer described by Firmani and Ruiz (1981), consisting of a WL30677 Westinghouse image intensifier described by Ruiz (1974) and a SIT intensified camera described by Solar (1977).

The spectra were taken with a 200 line mm^{-1} grating giving a resolution of about 8 A $channel^{-1}$ in the first order (5300 – 8300 A) and about 4 A in the second order (3800–5500 A). Wide entrance slits (1.5×16.5 and 3.5×16.5 arcsec) were used to obtain the spectra and a second slit 7 arcsec East was used alternatively for sky subtraction. Spectrophotometric standards from Stone (1977) were observed on the same nights for calibration. The journal of observation is given in Table 1.

To link the emission-line intensities to the continuum, the observed equivalent widths are given. In all cases, the continuum level has been fitted by eye, this being one of the sources of error in the measurement of emission-line intensities. The other sources of error

TABLE 1

JOURNAL OF OBSERVATIONS

Object	Date of Observation	Wavelength Range (Å)	Resolution (Å/channel)	Slit (arcsec)
II Zw 136	08/08/81	3800 – 5500	4.2	1.5 X 16.5
II Zw 136	13/08/81	5300 – 8300	8.3	1.5 X 16.5
NGC 985	14/10/82	4050 – 5950	4.2	3.5 X 16.5
Mkn 609	15/10/82	4400 – 5650	4.2	3.5 X 16.5
3C 120	15/10/82	4030 – 5550	4.2	3.5 X 16.5

(related to the first one) are the uncertainties in the estimation of the width of the broad wings, and of the degree of blending due to nearby lines. The errors given in Table 2 are estimated on the basis of extreme combinations of these three sources of error.

In what follows we shall analyze each object separately.

III. DISCUSSION AND RESULTS

a) *II Zw 136*

The spectrum of this typical Sy 1 galaxy was taken in two parts (Figure 1), the resolution is given in Table 1. Table 2 lists the values for line intensities and equivalent widths. Table 3 shows a comparison of width (FWHI and FWZI) measurements. From Table 3 and the comparison with previous determinations of the intensity in Hβ (Osterbrock 1977; Grandi 1981) we conclude that, within the error limits, the emission lines have not varied for this galaxy, at least over the time scale considered. The Balmer decrement is particularly smooth for this object.

b) *NGC 985*

This is one of the few ring galaxies known to have Seyfert characteristics. Line intensities and equivalent widths are given in Table 2. The spectrum is shown in Figure 2.

De Vaucouleurs and de Vaucouleurs (1985) classified this galaxy as Sy1. From Figure 2 one can clearly see a

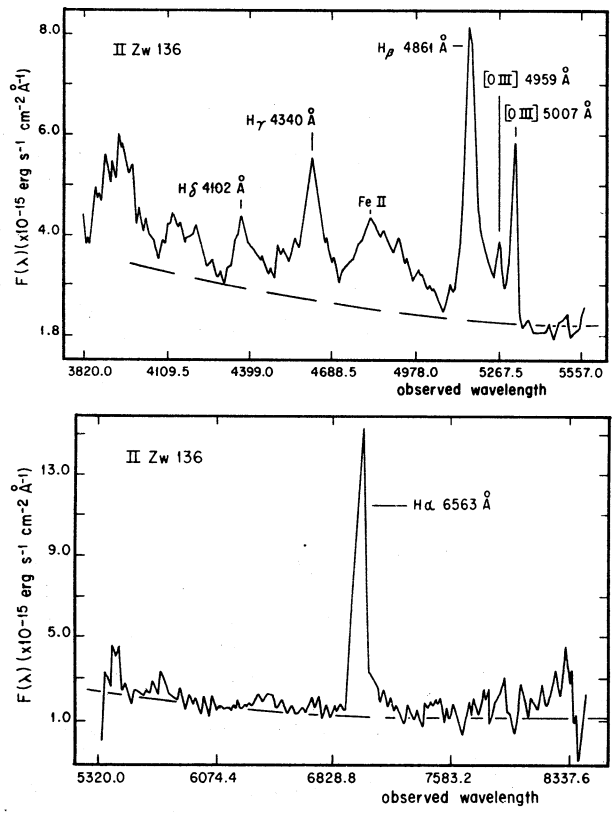

Fig. 1. Observed spectrum of II Zw 136 (*a*: blue, *b*: red).

TABLE 2

OBSERVED INTENSITIES AND EQUIVALENT WIDTHS[a]

			Hδ		Hγ		Hβ		[O III] 4959		[O III] 5007		Hα	
Object	z	m_V	I_o	W_o	I_o	W_o	I_o	W_o	I_o	W_o	I_o	W_o	I_o	W_o
II Zw 136	0.062	14.3	9 ± 3	30 ± 7	23 ± 4	85 ± 9	36 ± 3	156 ± 8	6 ± 0.3	25 ± 1	17 ± 0.5	50 ± 2	101 ± 3	565 ± 20
NGC 985	0.043	14.5	–	–	11 ± 2	38 ± 7	23 ± 5	81 ± 18	10 ± 2	36 ± 7	32 ± 1	73 ± 4	–	–
Mkn 609	0.032	14.5	–	–	–	–	2.2 ± 0.9	11 ± 4	2.3 ± 0.7	13 ± 2	7.1 ± 0.2	35 ± 1	–	–
3C 120	0.033	14.2	–	–	–	–	27 ± 4	90 ± 8	7 ± 1	30 ± 5	20 ± 2	83 ± 11	–	–

a. Observed intensities are given in units of 10^{-14} erg cm^{-2} s^{-1}. Observed equivalent widths in Å.

TABLE 3

FULL WIDTHS AT HALF MAXIMUM AND ZERO INTENSITY
FOR II Zw 136 (km s^{-1})

	Hα		Hβ	
	(1)	(2)	(1)	(2)
FWHM	2700 ± 200	2200 ± 300	2238 ± 300	2300 ± 400
FWZI	8571 ± 800	10100 ± 1000	11192 ± 1500	11400 ± 1900

1, This work.
2. Osterbrock (1977).

narrow component in Hβ, and the ratio [OIII]/Hβ does not correspond to a typical Sy1 galaxy. We believe that the type is certainly intermediate between Seyfert 1 and 2.

We have found a value of $\alpha_{opt} = -1.7 \pm 0.2$ for the spectral index of a power law continuum energy distribution in the wavelength range observed.

c) *Mkn 609*

This galaxy was first classified as a Sy1 by Weedman (1976) based only on morphological criteria. When the first high resolution spectra were obtained, Osterbrock (1978) classified it as intermediate type, Sy1.8. The superposition of a narrow component on broad wings in Hβ can be seen in our spectrum (Figure 3). Table 2 shows the intensities and equivalent widths for Hβ and [OIII]: these are the first absolute flux values reported for this galaxy.

d) *3C120*

This is a luminous Sy1 galaxy (often included in QSOs lists as well; z = 0.033), with a compact radio core. The morphology is most likely spiral (Arp 1975). 3C120 is highly variable at all wavelengths in which data have been collected. The optical nucleus is variable by almost two magnitudes on time-scales of years, with smaller changes occurring in days (Lyutyi 1979; Pollack *et al.* 1979). Similar behaviour is seen in the infrared (Rieke and Lebofsky 1979), in radio flux at different frequencies (Epstein *et al.* 1982 and references therein) and in X-rays (Halpern 1985). Perhaps the most interesting observational results are the *VLBI* maps of Walker *et al.* (1982, 1984) which show structural variations indicative of multiple ejection at apparent superluminal velocities. It is also well known that the line spectrum is highly variable, see. e.g. Oke, Readhead, and Sargent (1980).

The comparison of observations performed with different apertures, detectors, etc. is not the ideal approach to the study of variability, and thus, since the variability of line intensities is so well established for this galaxy,

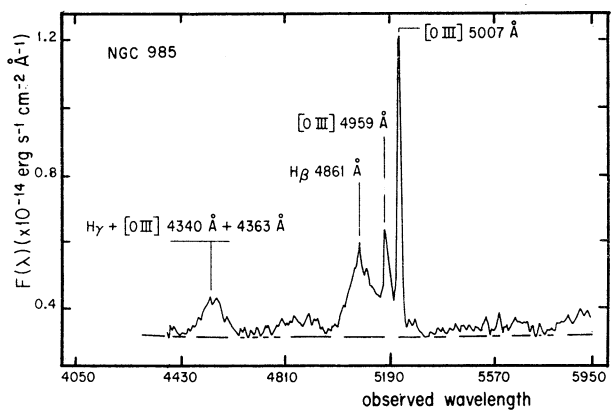

Fig. 2. Observed spectrum of NGC 985.

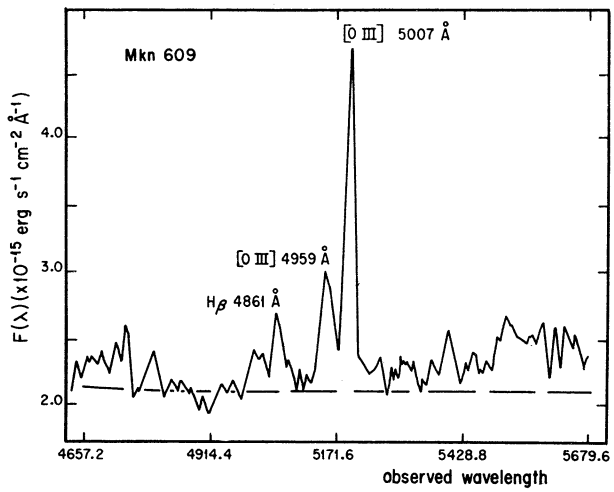

Fig. 3. Observed spectrum of Mkn 609.

we do not compare our values for intensities and equivalent widths (Table 2) with previous determinations.

The study of profile variation, has unfortunately been handicapped by the lack of high resolution spectra. Al-

though good profiles have not been published, evidence for variability of the Hβ profile can be inferred from Table 4, in which we compare measurements of FWZI and FWHM of Hβ by different authors (this work included). The type of variability deduced from Table 4 (a broadening of the upper part of the line) has not been found before. Since this effect refers to a broadening at half maximum, no continuum fitting effects can be important to bias the measurements.

TABLE 4

FULL WIDTHS OF Hβ AT HALF MAXIMUM AND ZERO INTENSITY FOR 3C 120 (km s^{-1})

	(1)	(2)	(3)
FWHM	2000	1200	3046 ± 200
FWZI	–	10000	9691 ± 700

1. Shields *et al.* (1972).
2. Oke and Zimmerman (1979).
3. This work.

We are grateful to S. Torres-Peimbert for a critical revision of the manuscript. We acknowledge G.F. Bisiacchi, L. Carrasco, C. Firmani, L. Solar, and A. Serrano for the development of the reduction software. This is Contribution No. 179 of Instituto de Astronomía, UNAM.

REFERENCES

Alloin, D., Pelat, D., Phillips, M.M., and Whittle, M. 1985, *Ap. J.*, **288**, 205.
Antokhin, I.I. and Bochkarev, N.G. 1984, *Astr. Zh.*, **60**, 448.
Arp, H. 1975, *Pub. A.S.P.*, **87**, 545.
Blandford, R.D. and McKee, C.F. 1982, *Ap. J.*, **255**, 419.
Capriotti, E., Foltz, C., and Peterson, B.M. 1982, *Ap. J.*, **261**, 35.
de Vaucouleurs, G. and de Vaucouleurs, A. 1975, *Ap. J.*, **197**, L1.
Epstein, E.E., Fogarty, W.G., Mottman, J., and Schneider, E. 1982, *A.J.*, **87**, 449.
Firmani, C. and Ruiz, E. 1981, in *Recent Advances in Observational Astronomy*, eds. H.L. Johnson and C. Allen (México: UNAM), p. 25.
Grandi, S.A. 1981, *Ap.J.*, **251**, 451.
Halpern, J.P. 1985, *Ap. J.*, in press.
Lyutyi, V.M. 1979, *Astr. Zh.*, **56**, 918.
Oke, J.B. and Zimmerman, B. 1979, *Ap. J.*, **232**, L13.
Oke, J.B., Readhead, A.C.S., and Sargent, W.L.W. 1980, *Pub. A.S.P.*, **92**, 758.
Osterbrock, D.E. 1977, *Ap. J.*, **215**, 733.
Osterbrock, D.E. 1978, *Phys. Scripta*, **17**, 137.
Pacholczyk, A.G. and Weymann, R.J. 1968, *A.J.*, **73**, 850.
Peterson, B.M., Foltz, C.B., Byard, P.L., and Wagner, R.M. 1982, *Ap. J. Suppl.*, **49**, 469.
Peterson, B.M., Foltz, C.B., Crenshaw, D.M., Meyers, K.A., and Byard, P.L. 1984, *Ap. J.*, **279**, 529.
Pollack, J.T., Pica, A.J., Leacock, R.J., Edwards, P.L., and Scott, R.L. 1979, *A.J.*, **84**, 1658.
Rieke, G.H. and Lebofsky, M.J. 1979, *Ap. J.*, **227**, 710.
Ruiz, E. 1974, Tesis profesional, Facultad de Ciencias, UNAM.
Shields, G.A., Oke, J.B., and Sargent, W.L.W. 1972, *Ap. J.*, **176**, 75.
Solar, A. 1977, Tesis profesional, Facultad de Ciencias, UNAM.
Stone, R.P.S. 1977, *Ap. J.*, **218**, 767.
Walker, R.C. *et al.* 1982, *Ap. J.*, **257**, 56.
Walker, R.C., Benson, J.M., Seielstad, G.A., and Unwin, S.C. 1984, in *IAU Symposium No. 110, VLBI and Compact Radio Sources*, eds. R. Fanti, R. Kellerman, and G. Setti (Dordrecht: D. Reidel), p. 121.
Weedman, D.W. 1976, *Ap. J.*, **208**, 30.

Deborah Dultzin-Hacyan and Miguel A. Herrera: Instituto de Astronomía, UNAM, Apartado Postal 70-264, 04510 México, D.F., México.
Noemí Núñez: Laboratorio de Física General, Departamento de Física, Facultad de Ciencias, UNAM, 04510 México, D.F., México.